

# Investigation the Impact of SnO<sub>2</sub> Additive on the Structural, Optical, Electrical and Gas Sensing Characteristics of LaCrO<sub>3</sub> Perovskite

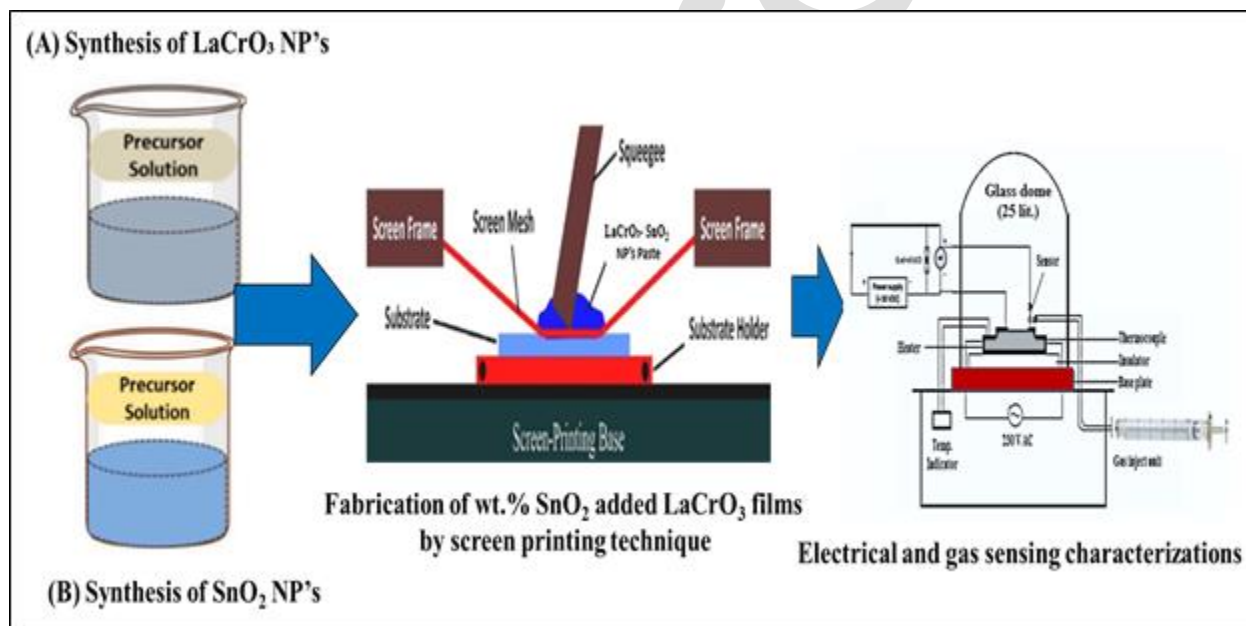
<sup>\*1</sup>Somnath Bhika Handge, <sup>2</sup>Uglal Pandit Shinde, <sup>3</sup>Dharma Kisan Halwar

<sup>1, 2, 3</sup> Research Centre in Electronic Science, Mahatma Gandhi Vidyamandir's Loknete Vyankatrao Hiray Arts, Science and Commerce College, Panchavati, Nashik-03, Affiliated to SPPU, Pune, Maharashtra - 422003, India.

<sup>2</sup>M.J.M. Arts, Commerce and Science College, Karanjali, Tal. Peth, Dist. Nashik, Affiliated to SPPU, Pune, Maharashtra - 422208, India.

Corresponding author: [somnathhandge@gmail.com](mailto:somnathhandge@gmail.com)

## Graphical Abstract



## Abstract

This study investigates the effect of SnO<sub>2</sub> as an additive on the structural, electrical, optical, and gas sensing properties of LaCrO<sub>3</sub> nanoparticles. SnO<sub>2</sub> is added into the LaCrO<sub>3</sub> by weight percentage (1 wt. %, 3 wt. %, 5 wt. %, 7 wt. %, 9 wt. % and 11 wt. %) employing screen printing method. Initially, the nanoparticles of SnO<sub>2</sub> and LaCrO<sub>3</sub> separately synthesis by sol-gel method and then used for the development of thick films. LaCrO<sub>3</sub> is used as host material while SnO<sub>2</sub> is

additive material. The structural characterizations like FESEM, EDX and XRD were carried out to investigate the morphology, elements and crystallite size respectively. The inclusion of SnO<sub>2</sub> modifies the crystalline structure and surface morphology of LaCrO<sub>3</sub>, as revealed by structural analyses. The optical characterizations like FTIR and UV were used for the study of impact of SnO<sub>2</sub> additive on functional group and band gap of the host material respectively. Optical studies indicate a modification in the bandgap, affecting light absorption properties and indicating changes in electronic transitions. The electrical characterizations were conducted by using half bridge method. Electrical resistivity measurements show enhanced performance, likely due to variation in charge carrier mobility induced by the SnO<sub>2</sub> additive. Among other selected wt. % SnO<sub>2</sub> additives, 9 wt. % SnO<sub>2</sub> added LaCrO<sub>3</sub> thick films shows maximum sensitivity to CH<sub>4</sub> gas at 120°C operating temperature. The gas sensing characteristics demonstrate enhanced sensitivity, selectivity, and response time to target gases, suggesting that SnO<sub>2</sub> doping improves the sensing capabilities of LaCrO<sub>3</sub> nanoparticles, making them more efficient as a gas sensor. Obtained findings suggest that, SnO<sub>2</sub> as an additive enhances the multifunctional properties of LaCrO<sub>3</sub> nanoparticles, making them promising candidates for advanced gas sensing applications.

**Keywords:** Additive, sol-gel, weight percentage, morphology crystalline structure, nanoparticles.

## 1. Introduction:

The incorporation of metal oxide additives in metal oxide semiconductors is vital for the sustainable development of the environment [1]. These additives enhance the efficiency of semiconductors in applications like air and water purification, renewable energy, and gas sensing technologies, all crucial for environmental protection [1, 2]. Metal oxide additives improve the catalytic properties of semiconductors, enabling more efficient breakdown of pollutants in air and water, thereby supporting cleaner ecosystems [2, 3]. In gas sensing, they enhance sensitivity and selectivity for detecting harmful gases, contributing to better air quality monitoring and pollution control [4, 5]. Metal oxide additives improve the energy efficiency of devices by enhancing charge carrier mobility and reducing energy consumption, supporting sustainable energy technologies such as solar cells and photocatalysts. The use of environmentally friendly and abundant metal oxides aligns with green chemistry principles, ensuring that the materials themselves are sustainable [5, 6]. Metal oxide additives in semiconductors play a crucial role in addressing

environmental challenges, promoting cleaner technologies, and contributing to the broader goals of sustainability [6, 7].

By introducing metal oxide additives, the electronic structure of the semiconductor is modified, leading to changes in bandgap energy, charge carrier concentration, and mobility. These improve the material's optical properties, such as light absorption and photoconductivity, making it more efficient in optoelectronic devices [7, 8]. Additives, on the other hand, significantly alter surface morphology, porosity, and active sites, which are critical for gas sensing performance. They enhance the adsorption and desorption of target gas molecules, improving sensitivity, selectivity, and response time. Additionally, dopants create oxygen vacancies or modify the oxidation states of metal ions, facilitating better interaction with gases and enhancing the sensing mechanism [8, 9]. According to literature survey, additives modify the structural, electrical, and surface properties of host metal oxide semiconductors, making them more effective for specific optical and gas sensing applications [7-10].

Lanthanum Chromite ( $\text{LaCrO}_3$ ) nanoparticles exhibit unique physicochemical properties, including a perovskite crystal structure, high thermal stability, and intrinsic p-type semiconducting behavior [11]. They possess a wide bandgap ( $\sim 3$  eV) and antiferromagnetic properties due to the  $\text{Cr}^{3+}$  ions. These nanoparticles are synthesized using various methods such as sol-gel, hydrothermal synthesis, co-precipitation, solid-state reactions, and microwave-assisted techniques, each offering control over particle size, morphology, and crystallinity [12, 13].  $\text{LaCrO}_3$  nanoparticles are widely applied in solid oxide fuel cells (SOFCs) as interconnect materials due to their stability and conductivity at high temperatures, and in gas sensors for detecting gases like oxidising and reducing [14, 15]. Additionally, they are used in catalysis for oxidation reactions, photocatalysis for environmental pollutant degradation, and in magnetic and spintronic devices due to their magnetic properties. The versatility of  $\text{LaCrO}_3$  nanoparticles makes them crucial for energy, environmental, and electronic applications [15, 16].

$\text{SnO}_2$  (Tin Oxide) nanoparticles possess distinctive physicochemical properties, including a wide bandgap ( $\sim 3.6$  eV), high transparency in the visible range, and excellent thermal and chemical stability [17, 18]. They exhibit n-type semiconducting behavior, with high electron mobility and strong sensitivity to environmental changes, making them ideal for applications in electronics and gas sensing. The surface of  $\text{SnO}_2$  nanoparticles has a high density of oxygen vacancies, enhancing their reactivity, particularly in gas adsorption and catalytic processes. Also

the addition of SnO<sub>2</sub> in perovskite materials plays a significant role in enhancing their structural, electrical, and functional properties [9, 18]. It is a wide-bandgap semiconductor, improves the conductivity and carrier mobility of the perovskite material by introducing additional charge carriers and reducing resistive losses. Structurally, SnO<sub>2</sub> acts as a stabilizing agent, modifying the grain size and morphology, which is improve crystallinity and surface uniformity. In optical applications, SnO<sub>2</sub> additive influence light absorption by tuning the bandgap of the perovskite, enhancing its performance in devices like solar cells and optoelectronic devices [18, 19]. In gas sensing, SnO<sub>2</sub> boosts the sensitivity and selectivity of perovskite materials by providing more active sites for gas molecule adsorption and improving the response time. It also enhances the durability of the material in harsh environments by increasing its chemical stability [20, 21].

The sol-gel method is a widely used technique for synthesizing nanoparticles due to its simplicity, versatility, and ability to control particle size and morphology [22]. This process involves the transition of a system from a liquid sol to a solid gel phase. Typically, metal alkoxides or metal salts are used as precursors, which undergo hydrolysis and condensation reactions to form a network of metal-oxide bonds. The sol-gel method offers precise control over composition, purity, and homogeneity of nanoparticles [22, 23]. It allows for the synthesis of nanoparticles with uniform size and shape at relatively low temperatures. The screen printing method is a widely employed technique for fabricating gas sensors due to its simplicity, scalability, and cost-effectiveness. In this process, a gas-sensitive material, typically in the form of a paste of MOS, is deposited onto a substrate through a patterned screen or stencil. The screen is made of a fine mesh, and the material is applied by spreading the paste across the mesh with a squeegee, allowing it to pass through open areas of the stencil, forming a uniform layer on the substrate [24-28].

This work has laid its prominence on investigate the impact of SnO<sub>2</sub> additive on the structural, optical, electrical and gas sensing characteristics of LaCrO<sub>3</sub> perovskite nanoparticles. All the data related to characterizations was interpreted and matched to enticement out the conclusion.

## 2 Experimental work

All AR grade chemicals were purchased from Modern Laboratories, Nashik, India. All these chemicals were utilized without any further purifications. In this work, we have synthesis LaCrO<sub>3</sub> and SnO<sub>2</sub> nanoparticles separately by using low cost sol gel approach.

## 2.1 Synthesis of LaCrO<sub>3</sub> nanoparticles

The LaCrO<sub>3</sub> nanoparticles was synthesized using the sol-gel method, starting with the dissolution of 0.07 moles of lanthanum nitrate [La (NO<sub>3</sub>)<sub>3</sub>], and 0.075 moles of chromium nitrate [Cr (NO<sub>3</sub>)<sub>3</sub>] in a minimal amount of distilled water. In a separate beaker, 0.09 moles of citric acid was dissolved in distilled water. Both solutions were then combined and heated at 90°C with continuous stirring on a magnetic stirrer for 3-4 hours. During this process, a colored sol was formed, which gradually transformed into a viscous liquid, indicating the formation of a gel. The obtained gel was initially dried under an IR lamp for 30-40 minutes, followed by crushing and grinding to obtain fine precursor particles. Finally, the dried powder was calcined at 600°C for 5–6 hours, leading to the formation of LaCrO<sub>3</sub> nanoparticles with improved crystallinity and phase purity.

## 2.2 Synthesis of SnO<sub>2</sub> nanoparticles

Initially, 50 mL of isopropyl alcohol was mixed with the Sn(Cl<sub>2</sub>)·2H<sub>2</sub>O solution, and the resulting mixture was stirred continuously for 3–4 hours to obtain a homogeneous solution. To adjust the pH of the solution to 8–9, 0.1 M NaOH solution was added drop by drop using a burette while maintaining constant stirring. The solution was then allowed to settle for 2 hours, with an additional 40 minutes of stirring before settling. The obtained precipitates were thoroughly washed with acetone and distilled water to remove impurities and were subsequently dried at 90°C. After that the dried precipitate powder was calcined at 600°C for 3 hours in the muffle furnace. Finally, White coloured SnO<sub>2</sub> nanoparticles were obtained.

## 2.3 Preparation of SnO<sub>2</sub>-LaCrO<sub>3</sub> thick films

After successfully synthesis of LaCrO<sub>3</sub> and SnO<sub>2</sub> nanoparticles by sol gel approach, synthesized nanoparticles of LaCrO<sub>3</sub> and SnO<sub>2</sub> were used to developed thick films. In the development of the thick films, LaCrO<sub>3</sub> was used as host material and SnO<sub>2</sub> was used an additive material. The SnO<sub>2</sub> additive was added in the weight percentage (1 wt. %, 3 wt. %, 5 wt. %, 7 wt. %, 9 wt. % and 11 wt. %) into the LaCrO<sub>3</sub>. The all thick films of SnO<sub>2</sub> added LaCrO<sub>3</sub> developed

by screen printing technique. All films were developed on rectangular glass substrates of size  $1.25 \times 2.5$  cm using the screen printing technique for thick film deposition. Prior to deposition, the glass substrates were thoroughly cleaned with double-distilled water and acetone and then dried under an IR lamp to remove any residual contaminants. A thixotropic paste was prepared using a 70:30 ratio of organic (ethyl cellulose) and inorganic (butyl carbitol acetate) materials to ensure proper viscosity and adhesion. The paste was then forced through a stencil onto the glass substrate using a screen printing setup, forming uniform thick films. After deposition, the films were initially dried under an IR lamp for 20-30 minutes at ambient temperature, followed by annealing in a muffle furnace at  $400^{\circ}\text{C}$  to enhance crystallinity and adhesion. The prepared thick films were then utilized for further characterizations and potential applications.

## 2.4 Characterizations techniques

The developed  $\text{SnO}_2$  added  $\text{LaCrO}_3$  ( $\text{SnO}_2\text{-LaCrO}_3$ ) thick films were characterized by standard tools such as FESEM, EDS, XRD, FTIR and UV-vis spectroscopy. All these characterizations were carried out at CIF and department of Physics, savitribai Phule Pune University, Pune. The Electrical and gas sensing characterizations of developed  $\text{SnO}_2$  added  $\text{LaCrO}_3$  thick films were carried out using homemade static electrical and gas sensing setup as shown in Fig. 1 [29, 30].

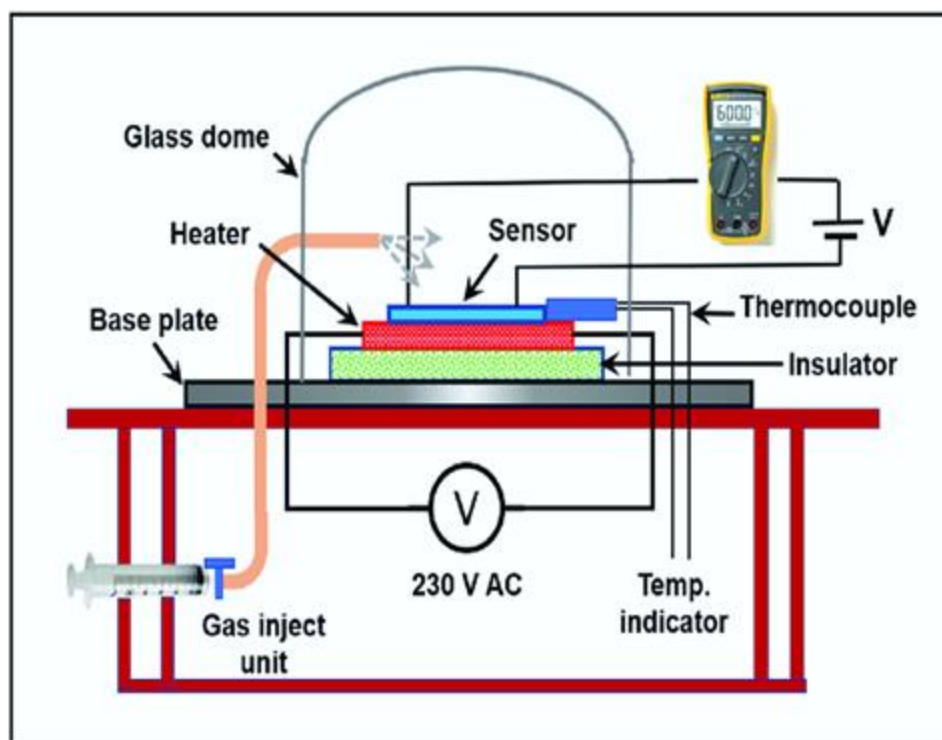


**Fig. 1.** Schematic diagram of static electrical and gas sensing characterizations system

### 3. Result and discussion

Field Emission Scanning Electron Microscopy (FESEM) combined with Energy-Dispersive X-ray Spectroscopy (EDS) is a powerful technique used for high-resolution imaging and elemental analysis of samples. The FESEM and EDS were performed on FEI NOVA SEM 450. Fig. 2 (a-f) shows FESEM micrographs of  $\text{SnO}_2$  added  $\text{LaCrO}_3$  thick films.

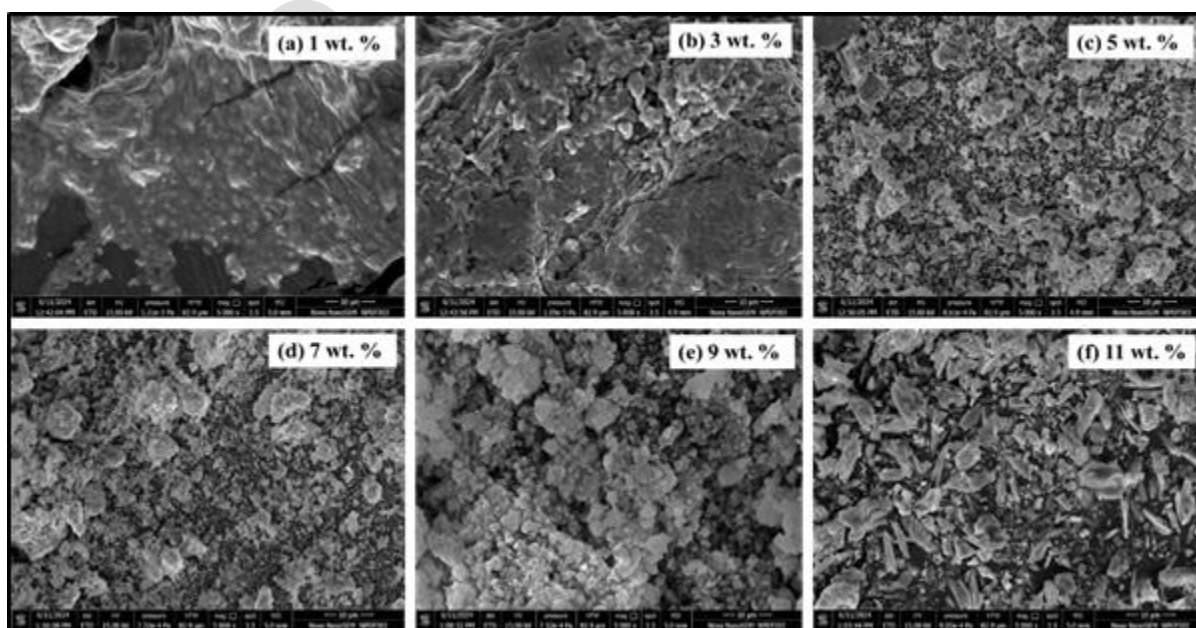


**Fig. 2.** FESEM micrograph of (a) 1 wt. %, (b) 3 wt. %, (c) 5 wt. %, (d) 7 wt. %, (e) 9 wt. % and (f) 11 wt. % SnO<sub>2</sub> added LaCrO<sub>3</sub> thick films

The FESEM micrographs reveal the presence of pores and voids within the film matrix. These voids enhance the surface area, providing numerous adsorption sites for gaseous molecules. In gas sensors, this increased porosity plays a crucial role as it allows the gas molecules to penetrate and interact with a larger portion of the material's surface [10, 29]. This interaction leads to more pronounced changes in the film's electrical properties upon gas exposure, thereby improving sensor response and sensitivity. Films also shows the agglomerates of SnO<sub>2</sub> particles dispersed within the LaCrO<sub>3</sub> matrix. Such particle clusters influence the surface morphology and impact the gas-sensing properties [8, 27]. While excessive agglomeration might limit the effective surface area due to particle clustering, moderate levels of aggregation can form channels and pathways that facilitate gas diffusion and enhance the overall sensing performance. Porosity is a key factor in determining gas sensing performance. The FESEM micrograph display varying porosity levels depending on the amount of SnO<sub>2</sub> added. High porosity ensures a larger surface area available for gas adsorption and reaction, leading to better sensitivity and faster sensor response times [10, 11]. It is also observed that, as the SnO<sub>2</sub> additive increases from lower percentages (1 wt. % to 7 wt. %), a gradual increase in porosity and void formation occurs due to the incorporation of SnO<sub>2</sub> into the LaCrO<sub>3</sub> matrix. However, at 9 wt. %, the concentration may reach an optimal point where SnO<sub>2</sub> particles begin to cluster and form networks, resulting in a more prominent porous microstructure. Beyond this concentration, such as at 11 wt. %, excessive SnO<sub>2</sub> may lead to particle agglomeration that fills available spaces, reducing overall porosity and void structure [30, 31]. The 9 wt. % SnO<sub>2</sub> added LaCrO<sub>3</sub> films exhibit a unique combination of enhanced porosity, more voids, and moderate particle agglomeration that collectively improve their suitability for applications such as gas sensing by maximizing surface interaction with analyte gases [32, 33]. The specific surface area (Sw) of films was measured using Brunauer-Emmett-Teller (BET) method (Eq. 1) [34, 35]. The measured specific surface area (Sw) of each sample is tabulated in Table 1.

$$Sw = \frac{6}{gd} \quad \text{Eq. 1}$$

Where,

Sw- Specific surface area, 6 –constant, d- diameter of spherical particle and g - composite density of material.

**Table 1.** Specific surface area of wt. % SnO<sub>2</sub> added LaCrO<sub>3</sub> films

<b>SnO<sub>2</sub>-LaCrO<sub>3</sub> Sample</b>	<b>Specific surface area (m<sup>2</sup>/g)</b>
1 wt. %	2.35
3 wt. %	3.24
5 wt. %	3.89
7 wt. %	4.12
9 wt. %	6.35
11 wt. %	4.89

The 9 wt.% SnO<sub>2</sub> added LaCrO<sub>3</sub> films exhibit a higher specific surface area compared to films with 1 wt.%, 3 wt.%, 5 wt.%, 7 wt.%, and 11 wt.% SnO<sub>2</sub> due to a unique combination of microstructural factors. A high specific surface area is beneficial for gas sensing, especially for CH<sub>4</sub>, as it provides a larger number of active sites for adsorption and reaction with methane molecules. When CH<sub>4</sub> comes into contact with the surface of the film, it interacts with adsorbed oxygen species, leading to a change in the electrical conductivity of the sensor material [34, 36].

EDS is often coupled with SEM and FESEM to perform elemental analysis of the sample. When the electron beam interacts with the sample, it emits characteristic X-rays that can be detected and analyzed to determine the elemental composition.

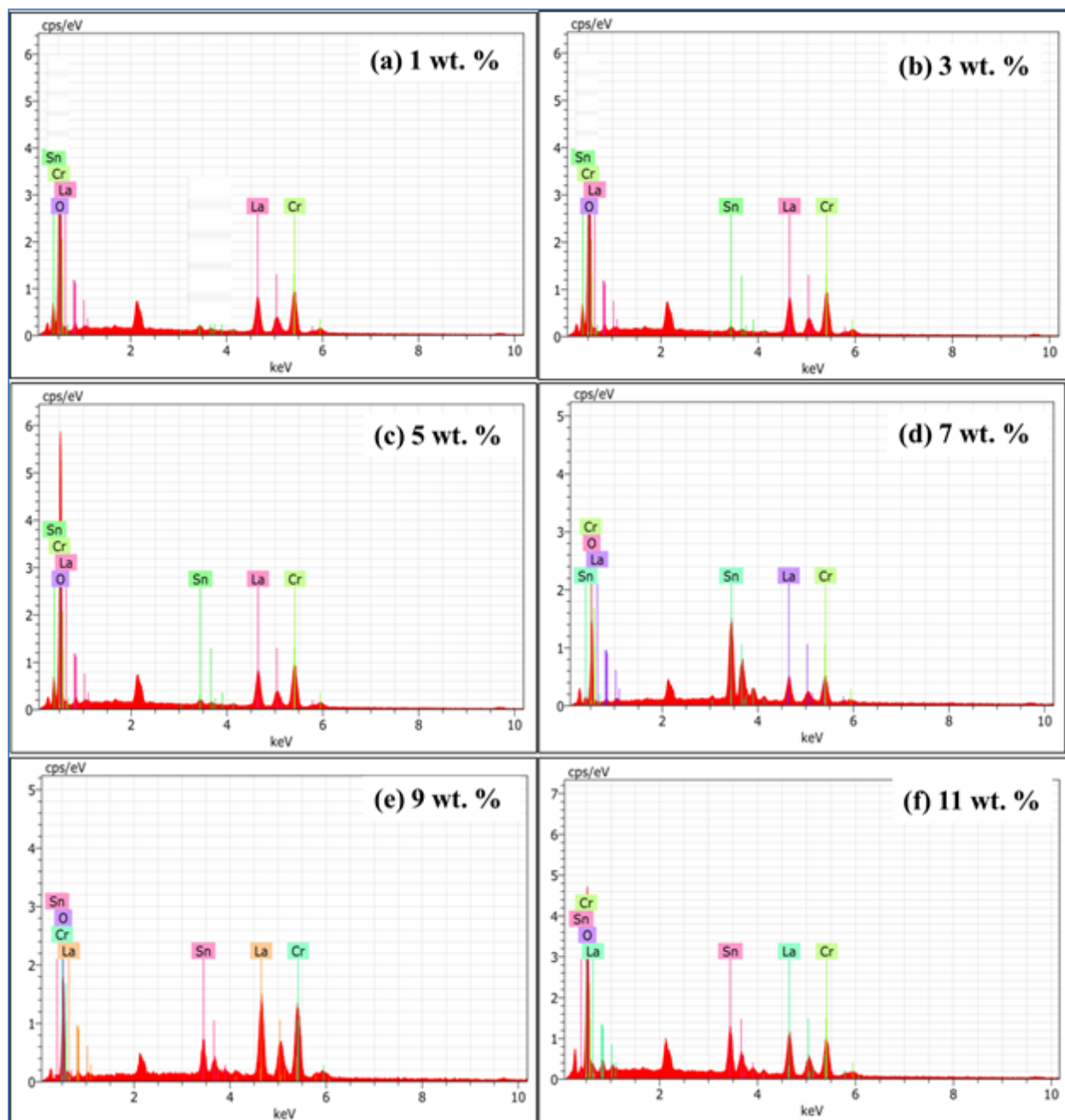


**Fig. 3.** EDS spectra of (a) 1 wt. %, (b) 3 wt. %, (c) 5 wt. %, (d) 7 wt. %, (e) 9 wt. % and (f) 11 wt. %  $\text{SnO}_2$  added  $\text{LaCrO}_3$  thick films

Fig. 3 (a-f) illustrations EDS spectra of  $\text{SnO}_2$  added  $\text{LaCrO}_3$  thick films. The lower oxygen content in terms of atomic percentage observed in 9 wt. %  $\text{SnO}_2$  added  $\text{LaCrO}_3$  films, as compared to films with 1 wt.%, 3 wt.%, 5 wt.%, 7 wt.%, and 11 wt.%  $\text{SnO}_2$  as shown Table 2. It is a beneficial attribute for gas sensing applications. The lower oxygen content in the 9 wt. %  $\text{SnO}_2$  added films suggests a higher concentration of oxygen vacancies. These vacancies are crucial for gas sensing

as they act as active sites that facilitate the adsorption and reaction of target gas molecules. The lower oxygen content observed in 9 wt. % SnO<sub>2</sub> added LaCrO<sub>3</sub> films promotes a higher concentration of oxygen vacancies, enhancing the reactivity, sensitivity, and responsiveness of the film toward gas molecules. This property makes it particularly beneficial for gas sensing applications by providing more active sites for adsorption, faster response times, and stronger signal changes during gas detection [36, 37].

**Table 2.** Elemental composition of prepared materials SnO<sub>2</sub> modified LaCrO<sub>3</sub> nanocomposite

SnO <sub>2</sub> -LaCrO <sub>3</sub> Sample	Elemental analysis Atomic (%)
1 wt.%	La – 47.87 Cr-15.36 Sn -11.25 O -25.52
3 wt.%	La – 49.12 Cr-12.36 Sn -13.25 O -25.27
5 wt.%	La – 52.05 Cr-10.24 Sn -14.05 O -23.66
7 wt.%	La – 49.79 Cr-11.24 Sn -16.11 O -22.86
9 wt.%	La – 48.59 Cr-11.69 Sn -17.91 O -21.81
11 wt.%	La – 43.93 Cr- 13.05 Sn -20.39 O -22.63

X-ray Diffraction (XRD) is a widely used analytical technique to determine the crystallographic structure, phase composition, and physical properties of materials. XRD is a fundamental tool for characterizing the structure and properties of crystalline materials in fields such as materials science, chemistry, geology, and solid-state physics. X-ray diffractometer [Bruker D8, Advance, Germany] using CuK $\alpha$  radiation ( $\lambda=1.5409$  Å) was used to examine the

structural properties of the developed  $\text{SnO}_2$  added  $\text{LaCrO}_3$  thick films. The obtained pattern of XRD of each sample was used to determine crystallite size and crystal structure of synthesized materials. In between the range of 20 and 80 degrees the XRD patterns were recorded for each sample. Fig. 4 (a-f) reveals the XRD pattern of  $\text{SnO}_2$  added  $\text{LaCrO}_3$  thick films.

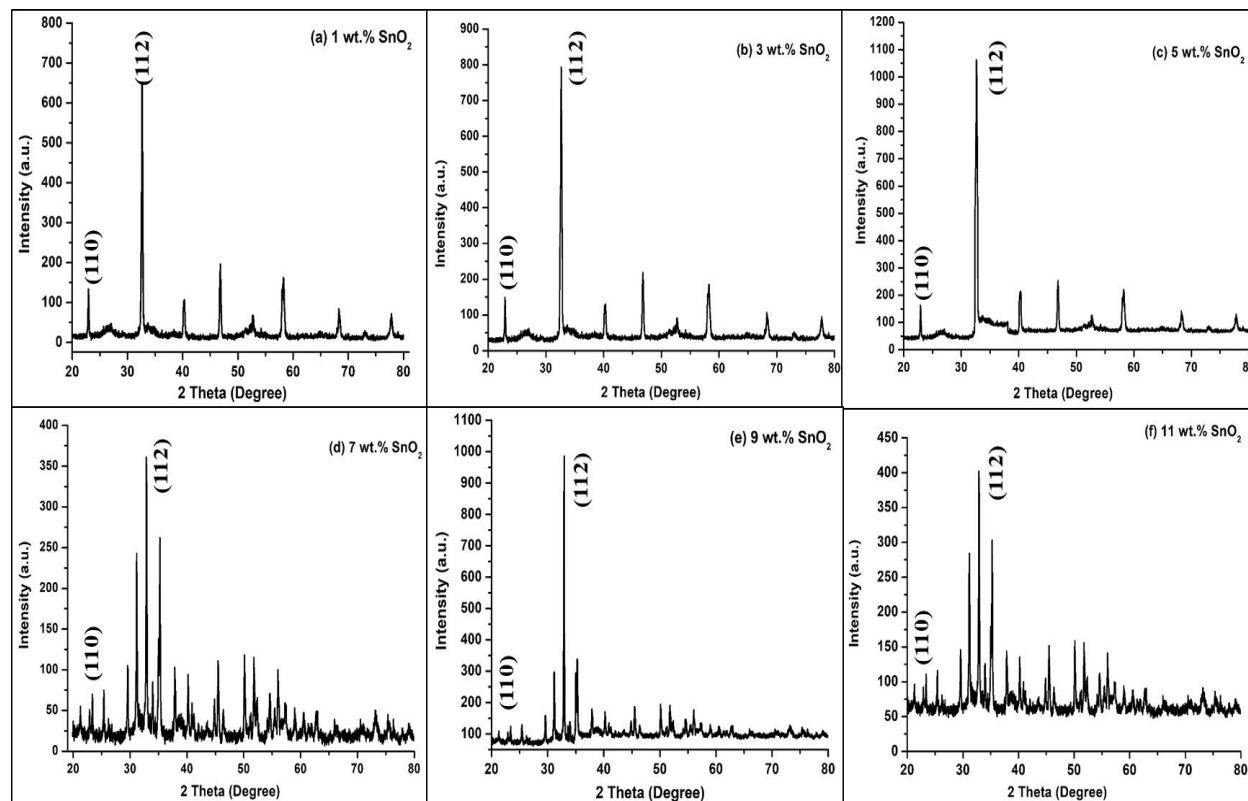


**Fig. 4.** XRD pattern of (a) 1 wt. %, (b) 3 wt. %, (c) 5 wt. %, (d) 7 wt. %, (e) 9 wt. % and (f) 11 wt. %  $\text{SnO}_2$  added  $\text{LaCrO}_3$  thick films

The XRD patterns wt. %  $\text{SnO}_2$  added  $\text{LaCrO}_3$  thick films exhibit characteristic peaks that compared with the standard JCPDS card numbers for  $\text{LaCrO}_3$  and  $\text{SnO}_2$ . Typically, the  $\text{LaCrO}_3$  phase is indexed using a specific JCPDS data card No. 24 -1016, indicating its orthorhombic structure [37, 38]. Similarly, peaks associated with  $\text{SnO}_2$  are often identified using JCPDS data card No. 41-1445, confirming the presence of  $\text{SnO}_2$  in its tetragonal rutile structure [39]. The prominent peak of  $\text{LaCrO}_3$  found to be at  $32.89^\circ$  indicate (112) miller plane while for  $\text{SnO}_2$  prominent peak found to be at  $21.86^\circ$  indicate (110) miller plane. Matching peaks to JCPDS standards ensures that the desired phases are present, and no unwanted phases or impurities are formed during synthesis. With increasing wt. %  $\text{SnO}_2$  content, there may be noticeable shifts in peak positions and changes in the intensity of the diffraction peaks. The incorporation of  $\text{SnO}_2$  into

the LaCrO<sub>3</sub> matrix lead to lattice distortions and changes in crystallite size [40, 41]. The 9 wt. % SnO<sub>2</sub> added LaCrO<sub>3</sub> films often show peak broadening due to reduced crystallite size, as confirmed by XRD analysis, indicating a more finely dispersed microstructure. The Debye-Scherrer's equation (Eq. 2) was used to determine the crystallite size [41, 42]. The calculated crystallite size of SnO<sub>2</sub> added LaCrO<sub>3</sub> thick films are tabulated in Table 3.

$$D = \frac{K\lambda}{\beta \cos\theta} \quad \text{Eq. 2}$$

Where,

D- Crystallite size, K – Constant (0.9–1),  $\beta$  - full-width half maxima (FWHM) and  $\theta$  - Angle of diffraction.

**Table 3.** Structural outcomes of SnO<sub>2</sub> added LaCrO<sub>3</sub> thick films from XRD.

SnO <sub>2</sub> -LaCrO <sub>3</sub> Sample	2 Theta (Degree)	FWHM (Degree)	Intensity (a.u)	Crystallite size (nm)
1 wt.%	32.64	0.2103	646.7	41.03
3 wt.%	32.70	0.2132	795.4	40.48
5 wt.%	32.65	0.2162	1067.9	39.91
7 wt.%	32.89	0.2216	360.6	38.97
9 wt.%	32.97	0.2418	990.8	35.72
11 wt.%	32.99	0.2396	404.3	37.99

The lower crystallite size observed in 9 wt.% SnO<sub>2</sub> added LaCrO<sub>3</sub> films, in comparison to films with 1 wt.%, 3 wt.%, 5 wt.%, 7 wt.%, and 11 wt.% SnO<sub>2</sub>. A lower crystallite size inherently leads to a higher surface area-to-volume ratio of the material. This increased surface area provides more active sites for the adsorption of gas molecules. In gas sensing applications. Gas sensing mechanisms in semiconducting oxides, such as SnO<sub>2</sub>-LaCrO<sub>3</sub> composites, rely on changes in electrical conductivity upon gas adsorption. The smaller crystallite size lead to improved charge carrier mobility across grain boundaries, enhancing the signal response of the sensor. This means that even small changes in gas concentration result in detectable variations in the electrical properties of the sensing film [41, 42]. The lower crystallite size of 9 wt.% SnO<sub>2</sub> added LaCrO<sub>3</sub> films offers a significant advantage for gas sensing by providing a higher surface area for adsorption, more active sites, enhanced charge carrier dynamics, and faster response times [43, 44]. Results reveals significant structural modifications due to the incorporation of SnO<sub>2</sub>. One of

the key observations is the gradual decrease in crystallite size with an increasing percentage of  $\text{SnO}_2$ . This reduction in crystallite size can be attributed to multiple factors. First, the substitution or incorporation of  $\text{Sn}^{4+}$  ions into the  $\text{LaCrO}_3$  lattice introduces lattice strain and distortion, which restricts crystal growth. The presence of  $\text{SnO}_2$  at higher concentrations hinders the mobility of  $\text{LaCrO}_3$  grains during annealing, thereby limiting their ability to coalesce and grow into larger crystallites. Another contributing factor is the possible formation of a secondary  $\text{SnO}_2$  phase, which disrupts the uniformity of  $\text{LaCrO}_3$  crystal growth and leads to more refined nanoscale grain formation. Moreover, increased doping introduces defects and oxygen vacancies, which further inhibit grain boundary movement, leading to finer crystallite sizes.

FTIR is an analytical technique used to identify and study chemical bonds and functional groups within materials by measuring their absorption of infrared light. FTIR is primarily used to identify the presence of specific functional groups in a sample by comparing absorption bands to known reference spectra. Fig. 5 (a-f) display the FTIR spectra of  $\text{SnO}_2$  added  $\text{LaCrO}_3$  thick films.

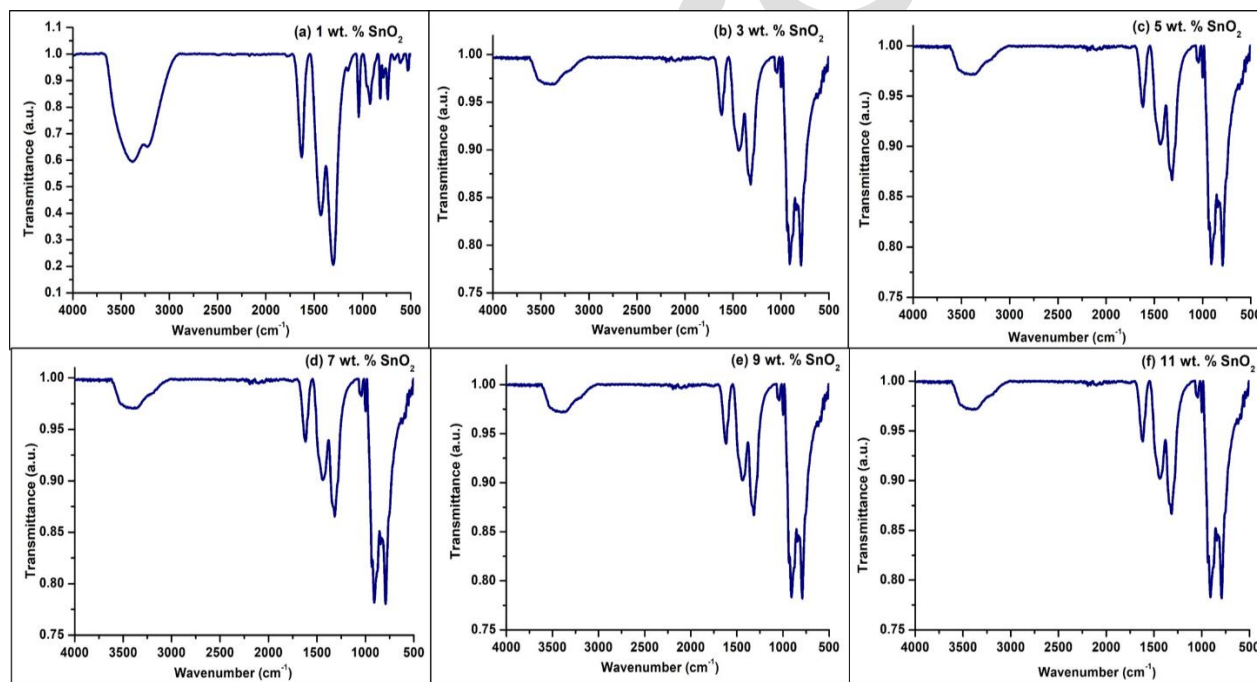


**Fig. 5.** FTIR spectra of (a) 1 wt. %, (b) 3 wt. %, (c) 5 wt. %, (d) 7 wt. %, (e) 9 wt. % and (f) 11 wt. %  $\text{SnO}_2$  added  $\text{LaCrO}_3$  thick films

The FTIR spectrum of  $\text{SnO}_2$  added  $\text{LaCrO}_3$  thick films typically exhibits characteristic absorption bands associated with metal-oxygen vibrations, such as La–O and Cr–O stretching and bending modes. These peaks are usually observed in the lower wavenumber region (below  $1000\text{ cm}^{-1}$ ).  $\text{LaCrO}_3$  peaks shows strong absorption bands at  $594.08\text{ cm}^{-1}$  for La – O stretch and

420.48  $\text{cm}^{-1}$  for Cr–O stretch. Peaks of Sn–O bonds from the  $\text{SnO}_2$  phase are typically observed around 500–700  $\text{cm}^{-1}$ . Peaks around 3200–3600  $\text{cm}^{-1}$  may correspond to O–H stretching vibrations if there is residual surface moisture or chemisorbed hydroxyl groups on the surface of the films [45, 46]. These groups play a role in gas sensing, as they may interact with target gas molecules. Fig. 5 (a–f) shows after  $\text{SnO}_2$  is introduced into the  $\text{LaCrO}_3$  matrix at different weight percentages, the vibrational peaks of La–O and Cr–O bonds may shift or change in intensity, indicating structural and bonding alterations. With increasing  $\text{SnO}_2$  content, shifts in the position of the La–O and Cr–O peaks may occur. These shifts suggest changes in bond strength and structural rearrangements due to the interaction of  $\text{SnO}_2$  with  $\text{LaCrO}_3$ . For example, the incorporation of  $\text{SnO}_2$  may introduce distortions in the lattice or create new bonding environments, leading to modified vibrational modes [34, 47]. Changes in oxygen-related vibrations are particularly relevant, as they influence the availability of oxygen species on the surface, which are useful for gas sensing reactions [37, 48].

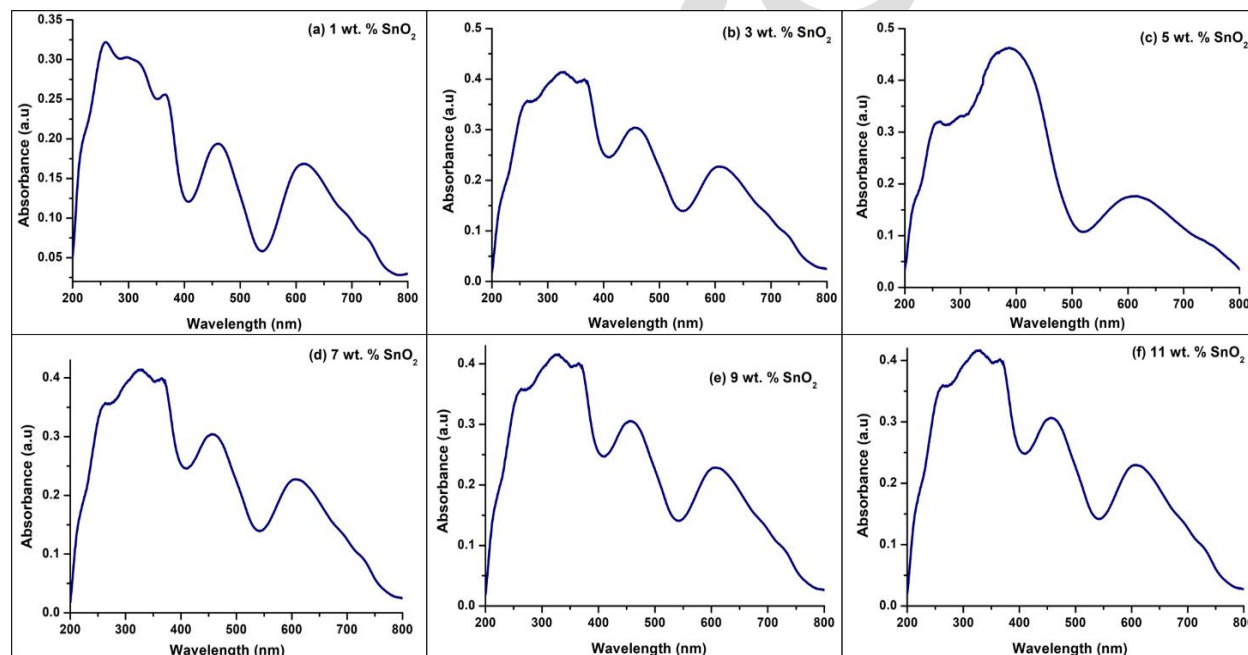


**Fig. 6.** Absorbance versus wavelength of (a) 1 wt. %, (b) 3 wt. %, (c) 5 wt. %, (d) 7 wt. %, (e) 9 wt. % and (f) 11 wt. %  $\text{SnO}_2$  added  $\text{LaCrO}_3$  thick films

UV-Visible spectroscopy is a widely utilized technique to study the optical properties of nanocomposites, providing essential information about their electronic structure, light absorption behavior, and bandgap energy. Fig. 6 (a–f) illustrate absorbance versus wavelength of  $\text{SnO}_2$  added  $\text{LaCrO}_3$  thick films. The absorbance versus wavelength spectra of  $\text{SnO}_2$  added  $\text{LaCrO}_3$  thick films

demonstrate significant variations in optical properties with changing SnO<sub>2</sub> content. The position of the absorption edge, the intensity of absorbance peaks, and the overall spectral profile are influenced by the interaction between LaCrO<sub>3</sub> and SnO<sub>2</sub>. These changes reflect modifications in electronic structure, light absorption behavior, and surface characteristics, making these films tunable for specific applications [44-47]. The absorbance spectra typically show a characteristic absorption edge that shifts with increasing SnO<sub>2</sub> content. As the SnO<sub>2</sub> wt. % increases, the absorption edge shifted and indicating changes in the bandgap energy of the composite films. The intensity of the absorbance spectra varies with the wt. % of SnO<sub>2</sub> added to the LaCrO<sub>3</sub> matrix. Lower concentrations (1 wt.% and 3 wt.%) may exhibit relatively lower absorbance, while moderate levels like 5 wt.% and 7 wt.% show increased intensity due to better integration and distribution of SnO<sub>2</sub> within LaCrO<sub>3</sub>. The 9 wt. % SnO<sub>2</sub> added film often displays enhanced absorbance, indicating strong light interaction due to the increased surface area and porosity provided by this composition. At 11 wt. % SnO<sub>2</sub>, a decrease in absorbance observed, potentially due to excessive SnO<sub>2</sub> leading to agglomeration, which enhanced the effective surface area. The energy band gap of SnO<sub>2</sub> added LaCrO<sub>3</sub> thick films is estimated using the Tauc plot method (Eq. 3), it is a common approach for determining the optical band gap of semiconductors and composite materials from their UV-Visible absorbance spectra [44-48].

$$(\alpha h\nu)^2 n = A (h\nu - E_g) \quad \text{Eq. 3}$$

Where,

$\alpha$  is the absorption coefficient of the material,  $h\nu$  is the photon energy (with  $h$  being Planck's constant and  $\nu$  being the frequency of light),  $A$  is a proportionality constant,  $E_g$  is the optical band gap energy, and  $n$  is an exponent that depends on the type of electronic transition.

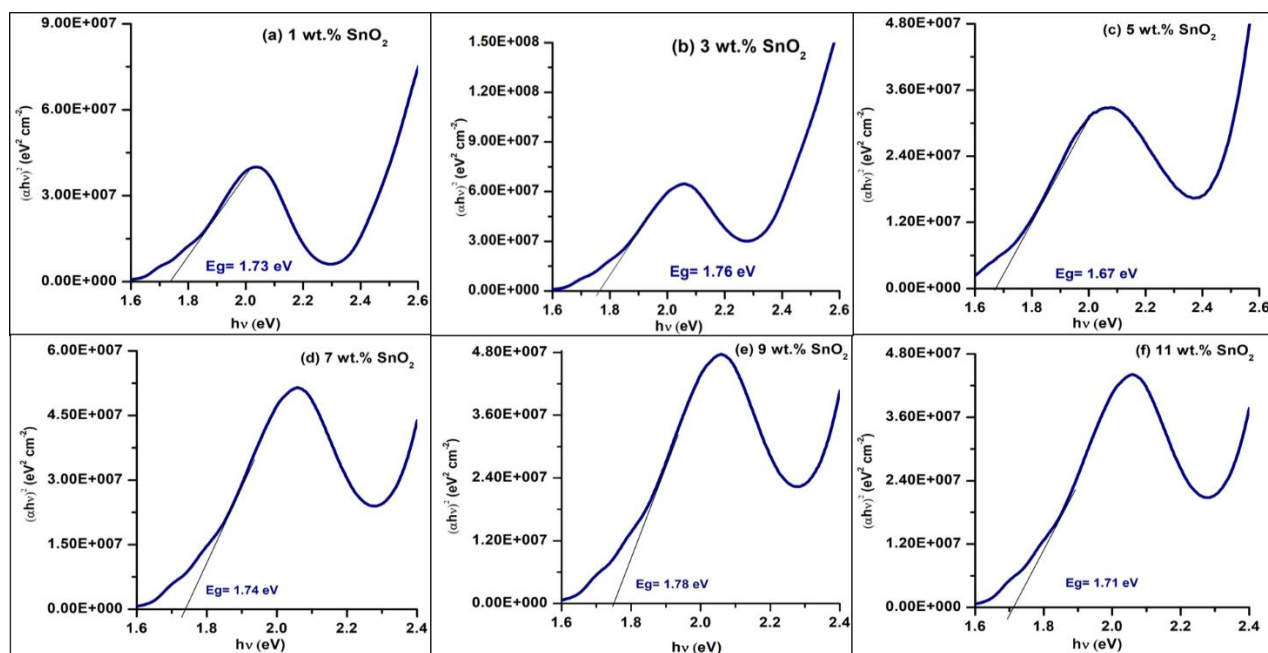


**Fig. 7.** Tauc plot of (a) 1 wt. %, (b) 3 wt. %, (c) 5 wt. %, (d) 7 wt. %, (e) 9 wt. % and (f) 11 wt. % SnO<sub>2</sub> added LaCrO<sub>3</sub> thick films

Fig. 7 (a-f) shows Tauc plot of SnO<sub>2</sub> added LaCrO<sub>3</sub> thick films. It is observed that, the incorporation of SnO<sub>2</sub> into the LaCrO<sub>3</sub> matrix modify the bandgap of the resulting films as shown inn Table 4. SnO<sub>2</sub>, a wide-bandgap semiconductor, influence the electronic structure of LaCrO<sub>3</sub>, leading to changes in the bandgap energy [47, 28].

**Table 4.** Energy band gap of wt. % SnO<sub>2</sub> added LaCrO<sub>3</sub> thick films.

SnO <sub>2</sub> -LaCrO <sub>3</sub> Sample	Energy band (eV)
1 wt. %	1.73
3 wt. %	1.76
5 wt. %	1.67
7 wt. %	1.74
9 wt. %	1.78
11 wt. %	1.71

The electric DC resistance of wt. % SnO<sub>2</sub> added LaCrO<sub>3</sub> thick films was measured using Eq. 4. The resistance versus temperature plots of wt. % SnO<sub>2</sub> added LaCrO<sub>3</sub> thick films are shown in Fig.11 (a-f).

$$R_{\text{sample}} = R_{\text{ref}} \left[ \frac{(V_{\text{supply}})}{(V_{\text{ref}})} - 1 \right] \quad \text{Eq. 4}$$

Where,  $R_{\text{sample}}$  is resistance of sample or film,  $R_{\text{ref}}$  is reference resistor (10M ohm),  $V_{\text{ref}}$  is reference voltage across the sample.

In the electrical characterizations we determined electrical parameters such as resistivity, activation energy at lower temperature region (LTR) and at higher temperature region (HTR) and temperature coefficient resistance (TCR) of  $\text{SnO}_2$  added  $\text{LaCrO}_3$  thick films by using Eqs. 5, 6 and 7 respectively [49, 50]. The obtained electrical parameters of  $\text{SnO}_2$  added  $\text{LaCrO}_3$  thick films are tabulated in Table 5. Fig. 8 (a-f) demonstrations resistance variation versus temperature plot wt. %  $\text{SnO}_2$  added  $\text{LaCrO}_3$  thick films. The resistance variation versus temperature plot of wt. %  $\text{SnO}_2$  added  $\text{LaCrO}_3$  thick films shows semiconducting behavior because of the thermally activated conduction mechanism, where increased temperature excites more charge carriers, reducing the material's resistance. The addition of  $\text{SnO}_2$  introduces donor states that increase free electron concentration, further enhancing the semiconductor's electrical conductivity with rising temperature [34, 39].

The electrical resistance decreases with increasing temperature as reveal in Fig. 8 (a-f), due to the thermally activated excitation of charge carriers (electrons or holes) across the bandgap. As the temperature rises, more electrons gain enough energy to jump from the valence band to the conduction band, increasing the number of free charge carriers available for conduction.  $\text{SnO}_2$  added  $\text{LaCrO}_3$  thick films, the addition of  $\text{SnO}_2$  may create oxygen vacancies or donor states in the conduction band, which further enhances the material's conductivity, especially at higher temperatures [35, 39].

The semiconducting behavior of films also be linked to the activation energy required for conduction. At high temperatures, the activation energy in the material (related to the energy needed to excite electrons to the conduction band) becomes apparent in the slope of the resistance-temperature curve. The resistance-temperature plot is fitted to an Arrhenius equation, which gives the activation energy, helping to confirm the semiconducting nature of the films [35]. In the form of  $\text{Log } R_c$  versus inverse of temperature plot activation energy is estimated by using Arrhenius equation (Eq. 6). Fig. 9 (a-f) illustrate  $\text{Log } R_c$  versus inverse of temperature plot (Arrhenius plot) of wt. %  $\text{SnO}_2$  added  $\text{LaCrO}_3$  thick films [35, 49].

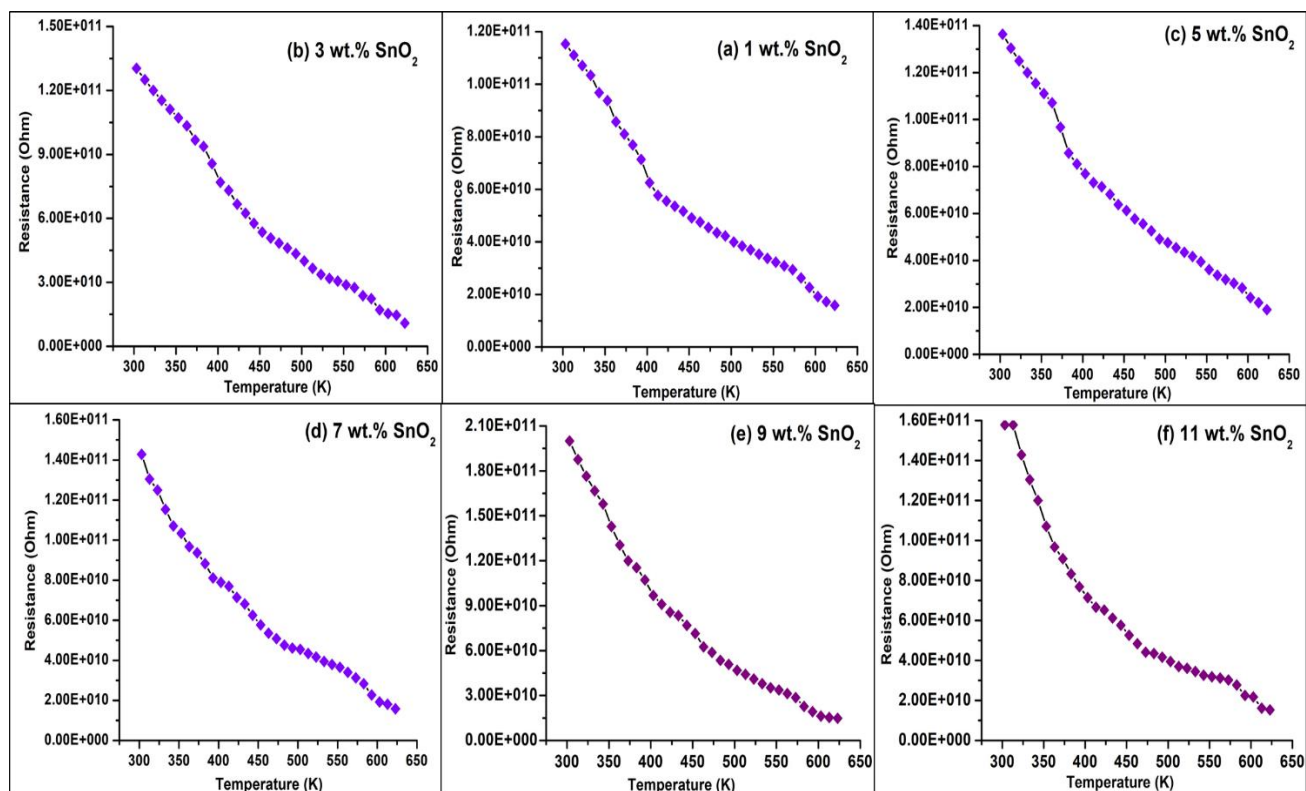


**Fig. 8.** Resistance variation versus temperature plot of (a) 1 wt. %, (b) 3 wt. %, (c) 5 wt. %, (d) 7 wt. %, (e) 9 wt. % and (f) 11 wt. %  $\text{SnO}_2$  added  $\text{LaCrO}_3$  thick films

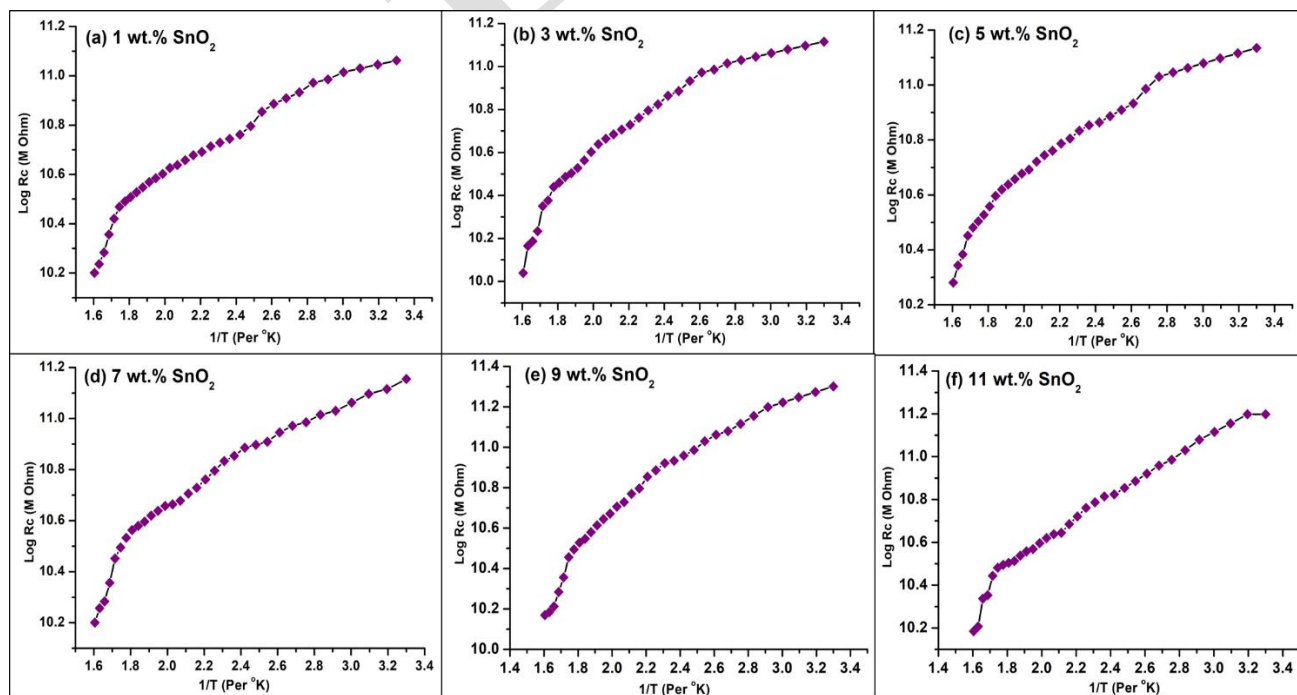


**Fig. 9.** Log  $R_c$  versus inverse of temperature plot of (a) 1 wt. %, (b) 3 wt. %, (c) 5 wt. %, (d) 7 wt. %, (e) 9 wt. % and (f) 11 wt. %  $\text{SnO}_2$  added  $\text{LaCrO}_3$  thick films

$$\rho = \left( \frac{R \times b \times t}{l} \right) \text{ ohm-m} \quad \text{Eq. 5}$$

Where,

R-Resistance of the film at room temperature, t- thickness of the film, b- breadth of the film, l - length of the film. Fig. 10 (a-c) indicate the wt. % SnO<sub>2</sub> additive versus thickness, resistivity and TCR plot of films.

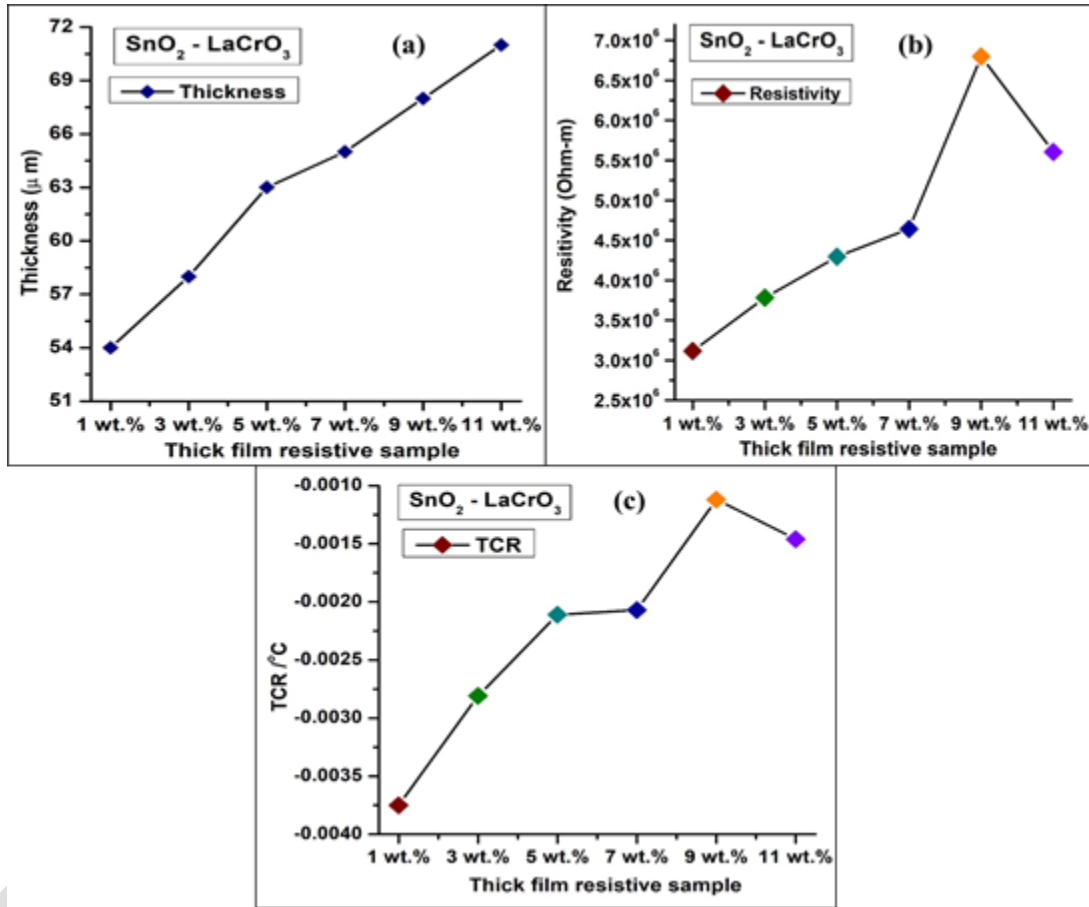


**Fig. 10.** Plot of (a) Thickness versus wt. % SnO<sub>2</sub> additive (b) Resistivity versus wt. % SnO<sub>2</sub> additive and (c) TCR versus wt. % SnO<sub>2</sub> additive thick films

$$\Delta E = \frac{\log R}{\log R_0} \times KT \quad \text{Eq. 6}$$

Where, ΔE-Activation energy, R-Resistance at room temperature, R<sub>0</sub>-Resistance at room temperature, K- Boltzmann constant and T-Absolute temperature.

$$TCR = \frac{1}{R_0} \left( \frac{\Delta R}{\Delta T} \right) / ^\circ C \quad \text{Eq. 7}$$

Where, ΔR-change in resistance between temperature T<sub>1</sub> and T<sub>2</sub>, ΔT-temperature difference between T<sub>1</sub> and T<sub>2</sub> and R<sub>0</sub>-Resistance of the film at room temperature.

The mass difference method is a straightforward and reliable technique employed for the measurement of the thickness of thin or thick films. This method is employ for the measurement of thickness of films. The thickness of all developed SnO<sub>2</sub> added LaCrO<sub>3</sub> thick films was estimated using Eq. 8 [34, 49].

$$\text{Thickness of film } (t) = \frac{\Delta M}{\rho A} \quad \text{Eq. 8}$$

Where,

$\Delta M$ - mass of the deposited film,  $\rho$ - composite density of the deposited material and A-area of the substrate covered by the film.

**Table 5.** Electrical parameters of SnO<sub>2</sub> added LaCrO<sub>3</sub> thick films.

SnO <sub>2</sub> -LaCrO <sub>3</sub> Sample	Thickness ( $\mu\text{m}$ )	Resistivity ( $\Omega\cdot\text{m}$ )	TCR ( $^{\circ}\text{C}$ )	Activation Energy (eV)	
				HTR	LTR
1 wt.%	54	3115114.6	-0.00375	0.0874	0.0486
3 wt.%	58	3782318.7	-0.00281	0.1656	0.0367
5 wt.%	63	4295139.5	-0.00211	0.1045	0.0382
7 wt.%	65	4642532.3	-0.00207	0.0648	0.0737
9 wt.%	68	6799660.1	-0.00112	0.1384	0.0531
11 wt.%	71	5604908.9	-0.00146	0.1371	0.4502

From Fig. 10 (a) shows as the wt. % SnO<sub>2</sub> additive increases in LaCrO<sub>3</sub> films, the thickness of the films increases in the range of 54 to 71 micrometers. It could be because of SnO<sub>2</sub> introduce additional nucleation sites during the deposition process, leading to thicker films as more material is deposited onto the glass substrate. Higher SnO<sub>2</sub> content could promote a greater number of nucleation centers, which in turn increases the thickness of film. A thicker film might be provides a larger surface area for interaction with gas molecules, which improve the gas adsorption capacity of film [49].

From Table 5, it is observed that, the 9 wt.% SnO<sub>2</sub> added LaCrO<sub>3</sub> films exhibiting maximum resistivity and temperature coefficient of resistance compared to 1 wt.%, 3 wt.%, 5 wt.%, 7 wt.%, and 11 wt.% SnO<sub>2</sub> added LaCrO<sub>3</sub> films. Resistivity refers to the material's ability to resist the flow of electric current, and in the case of SnO<sub>2</sub> added LaCrO<sub>3</sub> films, the 9 wt. % SnO<sub>2</sub> composition likely leads to a higher resistivity due to the specific balance between the SnO<sub>2</sub> donor electrons and the structural characteristics of LaCrO<sub>3</sub>. This high resistivity at room temperature is advantageous for gas sensing because it indicates that the material respond significantly to the

presence of gases. In many gas sensing applications, a material with a higher resistivity is more sensitive to changes in the gas atmosphere, particularly when the gas molecules interact with the surface of the film, causing changes in its electrical properties. These changes be detected and used to identify and quantify the target gas [35-37].

The TCR is a measure of how the resistivity of a material changes with temperature. A higher TCR indicates that the material's resistance changes more significantly with temperature variations, which is a critical factor in gas sensing. The 9 wt. % SnO<sub>2</sub> added LaCrO<sub>3</sub> films, the maximum TCR means that the film's resistance is more sensitive to temperature changes. This is particularly beneficial in temperature-modulated gas sensors, where the sensor operates by varying the temperature of the film to enhance the interaction between the material and the target gas molecules. A high TCR improves the sensor's response time and sensitivity because the change in resistance caused by the gas interaction will be more pronounced as temperature fluctuates. The combination of high resistivity and maximum TCR makes the 9 wt. % SnO<sub>2</sub> added LaCrO<sub>3</sub> films highly sensitive to small changes in gas concentration [35, 40]. When gases interact with the film, they alter its electronic structure, leading to measurable changes in resistance. A higher TCR means that these changes be detected more easily, even at low concentrations of gas.

In the gas sensing study we have investigated the impact of SnO<sub>2</sub> additive on the gas sensing properties of LaCrO<sub>3</sub> nanoparticles synthesized by sol gel method. On the basis of sensitivity, selectivity, response time, recovery time, limit of detection and reproducibility characterization the impact of SnO<sub>2</sub> additive on the gas sensing properties of LaCrO<sub>3</sub> were investigated. Sensitivity refers to the ability of the gas sensor to detect small changes in the concentration of the target gas [34, 49]. The sensitivity of wt. % SnO<sub>2</sub> added LaCrO<sub>3</sub> films is estimated by Eq. 9. Sensitivity versus operating temperature plot of SnO<sub>2</sub> added LaCrO<sub>3</sub> thick films is display in Fig. 11 (a-f). The sensitivity (S %) of SnO<sub>2</sub> added LaCrO<sub>3</sub> thick films was determined by using Eq. 9 [36, 40].

$$S(\%) = \frac{R_a - R_g}{R_a} \times 100 \quad \text{Eq. 9}$$

Where,

R<sub>a</sub> - Resistance of a thick film in air and R<sub>g</sub> - Resistance of thick film presence of target gas.

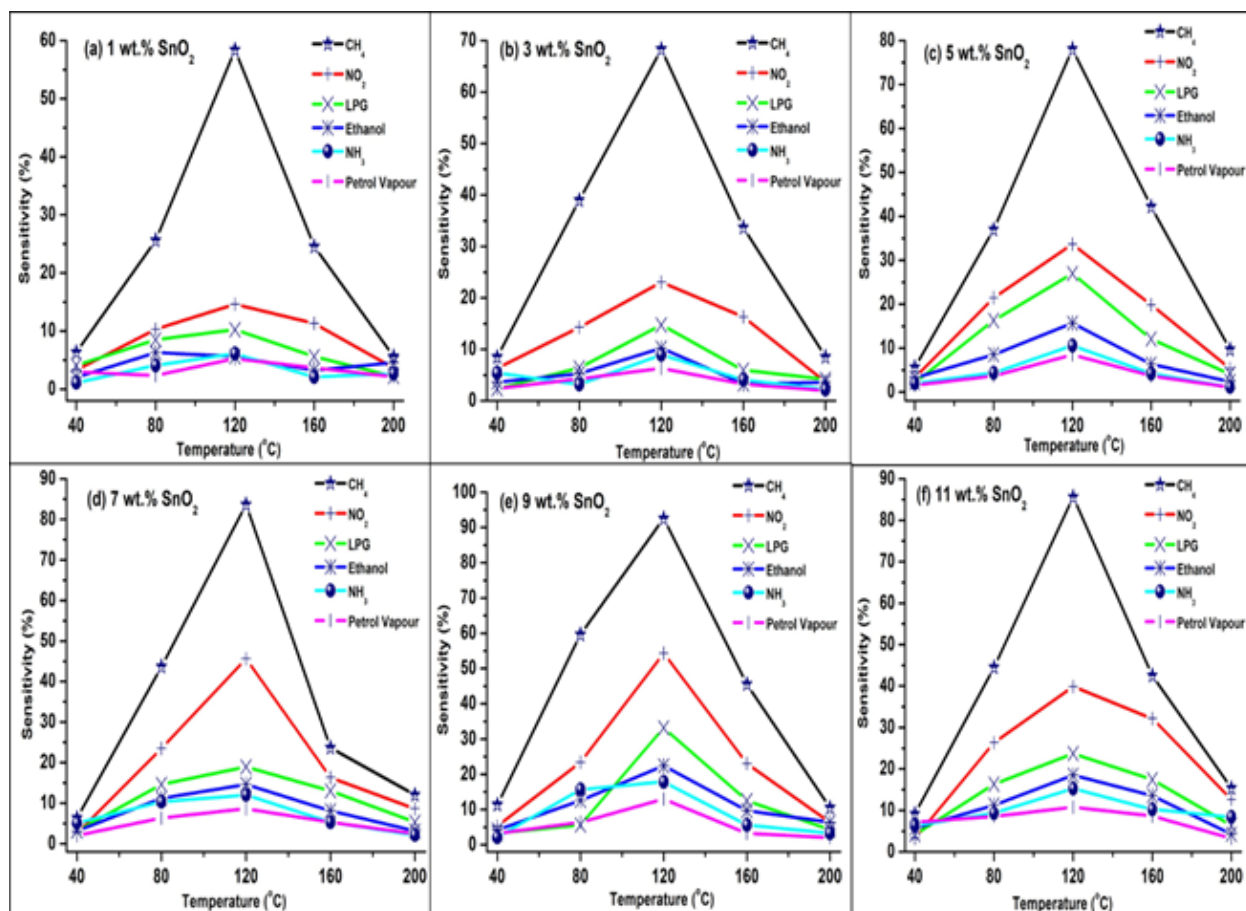


**Fig. 11.** Sensitivity versus operating temperature plot of (a) 1 wt. %, (b) 3 wt. %, (c) 5 wt. %, (d) 7 wt. %, (e) 9 wt. % and (f) 11 wt. %  $\text{SnO}_2$  added  $\text{LaCrO}_3$  thick films

Fig. 11 (a-f) shows the 9 wt.%  $\text{SnO}_2$  added  $\text{LaCrO}_3$  thick films show maximum sensitivity to  $\text{CH}_4$  gas at an operating temperature of  $120^\circ\text{C}$  and a gas concentration of 500 ppm compared to other targeted gases like ethanol,  $\text{NO}_2$ , LPG,  $\text{NH}_3$ , and petrol vapor. It is found that, the 9 wt.%  $\text{SnO}_2$  added  $\text{LaCrO}_3$  films demonstrate maximum sensitivity compared to the 1 wt.%, 3 wt.%, 5 wt.%, 7 wt.%, and 11 wt.%  $\text{SnO}_2$  added  $\text{LaCrO}_3$  films, making them highly beneficial for gas sensing applications. The addition of 9 wt. %  $\text{SnO}_2$  into  $\text{LaCrO}_3$  films creates a synergistic effect that enhances the interaction between the film and  $\text{CH}_4$  gas.  $\text{SnO}_2$  is known for its good semiconductor properties, which help increase the electronic conductivity of the composite film. The optimal  $\text{SnO}_2$  concentration likely results in a higher number of active sites on the surface of the film, which improves the adsorption and reaction of  $\text{CH}_4$  molecules, leading to a more significant change in the resistivity. Also the porous structure and increased surface area of the 9 wt. %  $\text{SnO}_2$  added  $\text{LaCrO}_3$  films provide a larger active surface for gas adsorption, making it more sensitive to

the presence of CH<sub>4</sub>. CH<sub>4</sub> molecules interact more effectively with the surface sites of the film, leading to a greater change in resistance upon exposure [36- 41].

The methane gas sensing mechanism of the prepared SnO<sub>2</sub>-added LaCrO<sub>3</sub> thick films is primarily governed by the surface adsorption and redox reactions occurring at the p–n heterojunction formed between p-type LaCrO<sub>3</sub> and n-type SnO<sub>2</sub>. When exposed to ambient air, oxygen molecules from the surroundings adsorb onto the film's surface, capturing free electrons from SnO<sub>2</sub> and forming negatively charged oxygen species (O<sub>2</sub><sup>-</sup>, O<sup>-</sup>, O<sup>2-</sup>). This process increases the depletion layer, leading to higher resistance. Upon exposure to CH<sub>4</sub> gas, methane molecules interact with these adsorbed oxygen species, undergoing oxidation reactions that release trapped electrons back into the conduction band [50-52]. This results in a reduction of the depletion layer and a corresponding decrease in resistance, which can be measured as a sensing signal. The presence of SnO<sub>2</sub> enhances the gas response by increasing the active surface area, providing more adsorption sites, and facilitating better charge carrier modulation at the SnO<sub>2</sub>- LaCrO<sub>3</sub> interface [26, 29]. The oxygen vacancies and defect states in the composite material improve catalytic activity, enhancing the selectivity and sensitivity toward CH<sub>4</sub> gas. This dynamic change in electrical resistance upon methane exposure forms the basis of the gas-sensing mechanism in SnO<sub>2</sub>-added LaCrO<sub>3</sub> thick films [53-56].

The maximum sensitivity to CH<sub>4</sub> gas was found to be 58.41, 68.32, 78.05, 83.66, 92.54 and 85.62% to 1 wt. %, 3 wt.%, 5 wt.%, 7 wt.%, 9 wt.%, and 11 wt.% SnO<sub>2</sub> added LaCrO<sub>3</sub> films respectively as shown in Fig. 12 (a). Selectivity refers to the ability of a gas sensor to respond to a specific target gas while minimizing the response to other gases present in the environment. It is crucial for sensors used in complex or multi-gas environments. It is estimated using Eq. 10.

$$\text{Selectivity} = \text{Response to target gas} / \text{Response to interferent gases} \quad \text{Eq. 10}$$

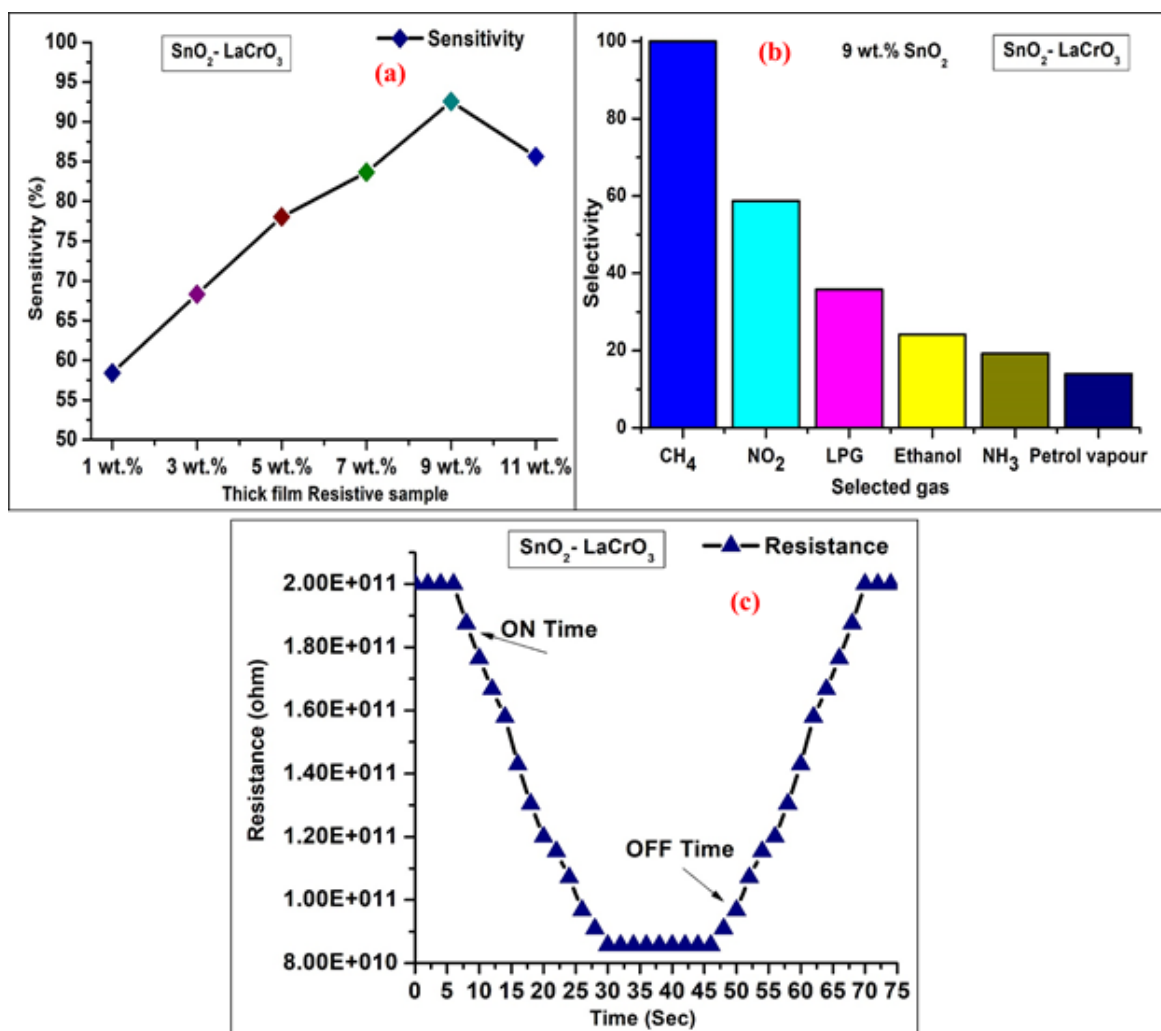


**Fig. 12.** Plot of (a) sensitivity versus wt. % SnO<sub>2</sub> additive (b) selectivity histogram of 9 wt. % SnO<sub>2</sub> added LaCrO<sub>3</sub> thick films (c) response and recovery time plot of 9 wt. % SnO<sub>2</sub> added LaCrO<sub>3</sub> thick films

Fig. 12 (b) shows the selectivity histogram of to CH<sub>4</sub> gas. The 9 wt.% SnO<sub>2</sub> added LaCrO<sub>3</sub> films show maximum selectivity to CH<sub>4</sub> gas when compared to 1 wt.%, 3 wt.%, 5 wt.%, 7 wt.%, and 11 wt.% SnO<sub>2</sub> added LaCrO<sub>3</sub> films. The 9 wt. % SnO<sub>2</sub> films exhibit an optimal porous structure, which increases the surface area available for gas adsorption. This high surface area facilitates the selective adsorption of CH<sub>4</sub> gas molecules while minimizing the adsorption of other interfering gases. The porous nature provides more active sites for CH<sub>4</sub>, ensuring that the film reacts more strongly with CH<sub>4</sub> compared to other gases, which contributes to better selectivity. Also lower SnO<sub>2</sub> additive concentrations may result in insufficient porosity, while higher SnO<sub>2</sub> concentrations

could lead to clustering or agglomeration, reducing the film's effective surface area and selectivity [37, 41].

Response time is the time taken by the sensor to reach a significant percentage (usually 90–95%) of its final response when exposed to the target gas [37]. Recovery time is the time required for the sensor to return to its baseline signal after being exposed to the target gas [49]. The 9 wt. %  $\text{SnO}_2$  added  $\text{LaCrO}_3$  films demonstrate a response time of 10 seconds and a recovery time of 51 seconds when exposed to  $\text{CH}_4$  gas. The 9 wt. %  $\text{SnO}_2$  concentration offers an optimal balance that enhances both response and recovery due to its tailored porosity, specific surface area, and favorable electronic properties, making it highly effective for methane detection compared to other  $\text{SnO}_2$  concentrations [28, 49].

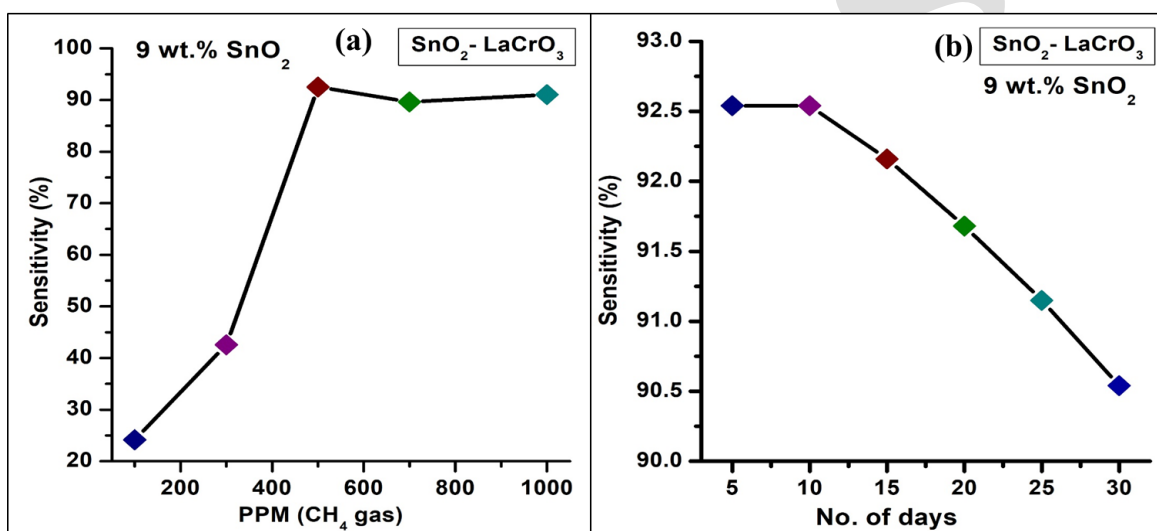


**Fig. 13.** Plot of (a) sensitivity versus  $\text{CH}_4$  gas concentration in ppm (b) Reproducibility graph for  $\text{CH}_4$  gas of 9 wt. %  $\text{SnO}_2$  added  $\text{LaCrO}_3$  thick films

The limit of detection (LOD) is the lowest concentration of the target gas that the sensor reliably detect. The lower the LOD, the more sensitive the sensor is to detecting trace amounts of the target gas, which is crucial for applications requiring early detection of harmful gases. Fig. 13 (a) shows the plot of sensitivity versus  $\text{CH}_4$  gas concentration in ppm. The 9 wt. %  $\text{SnO}_2$  added  $\text{LaCrO}_3$  films show maximum sensitivity to  $\text{CH}_4$  gas at a concentration of 500 ppm, compared to other concentrations such as 100 ppm, 300 ppm, 700 ppm, and 1000 ppm. It could be because of at 500 ppm, the concentration of  $\text{CH}_4$  gas creates an ideal balance for interaction with the 9 wt. %  $\text{SnO}_2$  added  $\text{LaCrO}_3$  films. The active sites on the film's surface are sufficiently occupied by  $\text{CH}_4$  molecules, leading to a maximum change in electrical resistance, which translates to peak

sensitivity. At lower concentrations 100 ppm and 300 ppm, there may be insufficient coverage of CH<sub>4</sub> molecules on the sensor surface [49, 50]. This limited interaction results in a smaller change in resistance, reducing the sensor's sensitivity. At higher concentrations 700 ppm and 1000 ppm, the surface may become saturated with CH<sub>4</sub> molecules. When saturation occurs, adding more gas does not significantly increase the resistance change, leading to a plateau or even a decline in sensitivity due to limitations in the number of available active sites for further adsorption [57].

Reproducibility refers to the ability of the gas sensor to produce consistent results under the same experimental conditions over multiple measurements. This includes consistency in response, stability, and signal variation. High reproducibility ensures that the developed films sensor is provide reliable and repeatable readings, which is essential for long-term monitoring and industrial applications where precision is critical. Fig. 13 (b) shows reproducibility plot of 9 wt. % SnO<sub>2</sub> added LaCrO<sub>3</sub> films. The decrease in sensitivity of 9 wt. % SnO<sub>2</sub> added LaCrO<sub>3</sub> films after 15 to 30 days is primarily due to surface contamination, structural degradation, environmental influences, and aging effects [39, 50]. These factors reduce the availability of active sites and impact the sensor's reactivity and charge transfer efficiency. Table 6 shows the reproducibility test of 9 wt. % SnO<sub>2</sub> added LaCrO<sub>3</sub> films.

**Table 6.** Reproducibility test of 9 wt. % SnO<sub>2</sub> added LaCrO<sub>3</sub> films

No. of day's	Sensitivity (%)
5	92.54
10	92.54
15	92.16
20	91.68
25	91.15
30	90.54

## Conclusions

In this study, SnO<sub>2</sub> and LaCrO<sub>3</sub> nanoparticles were successfully synthesized using the sol-gel method, and SnO<sub>2</sub>-added LaCrO<sub>3</sub> thick films were developed on glass substrates using a cost-effective screen printing technique. The impact of SnO<sub>2</sub> addition on the structural, optical, electrical, and gas-sensing properties of LaCrO<sub>3</sub> was systematically analyzed. The results revealed that the incorporation of SnO<sub>2</sub> significantly modified the microstructure, crystallite size, surface porosity, and electrical characteristics, leading to enhanced CH<sub>4</sub> gas sensing performance. Notably,

the 9 wt. % SnO<sub>2</sub>-doped LaCrO<sub>3</sub> films exhibited the highest sensitivity, selectivity, and fast response (10s) and recovery time (51s), making them highly effective for methane detection. FTIR and UV-Vis analyses confirmed modifications in vibrational and optical properties, correlating with improved charge transport and gas adsorption. The findings highlight the potential of SnO<sub>2</sub>-LaCrO<sub>3</sub> composites for high-performance gas sensors, demonstrating their suitability for real-world sensing applications.

## Declaration of Competing Interest

We declare that, we have not received any funding for the research work and we have no conflict of interest for our research work.

## Acknowledgment

The authors thank to Principal and Head of Research Centre in Electronic Science, Mahatma Gandhi Vidyamandir's Loknete Vyankatrao Hiray Arts, Science and Commerce College, Panchavati, Nashik-03 India, for providing laboratory facilities. The authors also acknowledge and pay sincere thanks to Head, Department of Physics and CIF S. P. Pune University, Pune for providing the laboratory facilities for FESEM, EDS, UV, FTIR and XRD characterization for present research work.

## References

1. Li Fu, Shixi You, Guangjun Li, Xingxing Li, and Zengchang Fan, "Application of Semiconductor Metal Oxide in Chemiresistive Methane Gas Sensor: Recent Developments and Future Perspectives", *Molecules*, 28, 2023, no. 18, 6710.
2. Naveen Kumar Elumalai, Chellappan Vijila, Rajan Jose, Ashraf Uddin, Seeram Ramakrishna, "Metal oxide semiconducting interfacial layers for photovoltaic and photocatalytic applications" *Materials for renewable and sustainable energy*, 4, 2015, 1-25
3. Yogendra K. Gautam, Kavita Sharma, Shrestha Tyagi, Anit K. Ambedkar, Manika Chaudhary and Beer Pal Singh, "Nanostructured metal oxide semiconductor-based sensors for greenhouse gas detection: Progress and challenges", *Royal Society open science*, 8, 2021, no.3, 201324.

4. Mehran Dadkhah and Jean-Marc Tulliani, "Nanostructured metal oxide semiconductors towards greenhouse gas detection", *Chemosensors*, 10, 2022, no. 2, 57.
5. Kurugundla Gopi Krishna, Saidireddy Parne, Nagaraju Pothukanuri, Velavan Kathirvelu, Suman Gandhi, and Dhananjay Joshi "Nanostructured metal oxide semiconductor-based gas sensors: A comprehensive review", *Sensors and Actuators A: Physical*, 341, 2022, 113578.
6. Maria Vesna Nikolic, Vladimir Milovanovic, Zorka Z. Vasiljevic and Zoran Stamenkovic "Semiconductor gas sensors: Materials, technology, design, and application", *Sensors*, 20, 2020, no.22, 6694.
7. Bilge Saruhan, Roussain Lontio Fomekong and Svitlana Nahirniak, "Influences of semiconductor metal oxide properties on gas sensing characteristics", *Frontiers in Sensors*, 2, 2021, 657931.
8. Tao Li, Wen Yin, Shouwu Gao, Yaning Sun, Peilong Xu, Shaohua Wu, Hao Kong, Guozheng Yang, and Gang Wei, "The combination of two-dimensional nanomaterials with metal oxide nanoparticles for gas sensors: a review" *Nanomaterials*, 12, 2022, no.6, 982.
9. Yushu Shi, Huiyan Xu, Tongyao Liu, Shah Zeb, Yong Nie , Yiming Zhao, Yiming Zhao, Chengyuan Qin, and Xuchuan Jiang, "Advanced development of metal oxide nanomaterials for H<sub>2</sub> gas sensing applications", *Materials Advances*, 2, 2021, no.5, 1530-1569.
10. David Degler, Udo Weimar and Nicolae Barsan, "Current understanding of the fundamental mechanisms of doped and loaded semiconducting metal-oxide-based gas sensing materials", *ACS sensors*, 4, 2019, no. 9, 2228-2249.
11. M. Coskun, O. Polat, F. M. Coskun, Z. Durmus, M. Caglar, and A. Turut "Synthesis, characterization and wide range frequency and temperature dependent electrical modulus study of LaCrO<sub>3</sub> and cobalt (Co) doped LaCrO<sub>3</sub> perovskite compounds", *Materials Science and Engineering: B*, 248, 2019, 114410.
12. Aref A A Qahtan, Naima Zarrin, Mehroosh Fatema, Hamdan A S Al-Shamiri, Wasi Khan and Shahid Husain, "A brief review on rare-earth chromites: synthesis, properties and applications", *Physica Scripta*, 99, 2024, no. 7, 072001.
13. Khan, Afroz, Hafiz, Mohammad, Gupta, Jhalak, Cheong, Jun Young, Zaid, M., Abushad, M., Fahad, Mohd and Hasan, Z , " Influence of Ni doping on microstructural, optical and

dielectric properties of lanthanum-based chromite” *Physica B: Condensed Matter*, 696, 2025, 416614.

14. Mariam Akram, Malika Rani, Rubia Shafique, Kiran Batool, Mohamed A. Habila, and Mika Sillanpää,” Fabrication of  $\text{LaCrO}_3@ \text{SiO}_2$  nanoparticles supported with graphene-oxide for capacitive energy storage and photocatalytic degradation applications”, *Journal of Inorganic and Organometallic Polymers and Materials*, 34, 2024, no. 1, .361-373.
15. S. M. El-Sheikh and M. M. Rashad, “Effect of  $\text{Sm}^{3+}$  and  $\text{Sr}^{2+}$  dopants on the FT-IR, photoluminescence and surface texture of lanthanum chromite nanoparticles”, *Journal of alloys and compounds*, 496, 2010, no. (1-2), 723-732.
16. Morteza Enhessari, Ali Salehabadi, Ashma Khoobi and Razie Amiri, “. Kinetic properties and structural analysis of  $\text{LaCrO}$  nanoparticles”, *Materials Science-Poland*, 35, 2017, no. 2, 368-373.
17. Ahmad A. Ahmad, A.B. Migdadi, and Qais M. Al-Bataineh, “Structural, optical, and electrical properties of strontium-doped tin dioxide films for high photoconductivity”, *Thin Solid Films*, 796, 2024, 140312.
18. Gauravkumar H. Patel, Sunil H. Chaki, Rohitkumar M. Kannaujiya, Zubain R. Parekh, Anilkumar B. Hirpara, Ankurkumar J. Khimani, and M. P. Deshpande, “Sol gel Synthesis and thermal Characterization of  $\text{SnO}_2$  nanoparticles”, *Physica B: Physics of Condensed Matter*, 613, 2021, 412987.
19. Aashish Kumar, Manan Bhasin, and Manasi Chitkara, “Morphological analysis and grain size distribution of  $\text{SnO}_2$  nanoparticles via digital image processing across diverse calcination temperatures”, *Journal of Microscopy*, 292, 2023, no. 3, 123-134.
20. Kaimo Deng, Qingjua Chen, and Liang Li, “Modification Engineering in  $\text{SnO}_2$  Electron Transport Layer toward Perovskite Solar Cells: Efficiency and Stability”, *Advanced Functional Materials*, 30, 2020, no. 46, 2004209.
21. Mohamad Saad, Puteri Sarah, Mohamad Saad, Puteri Sarah Aiman Aziz, Anees Hashim, and Hashimah, “Amorphous Phase of  $\text{SnO}_2$  doped  $\text{Al}_2\text{O}_3$  thin film: Optical and Structural Properties”, *ESTEEM Academic Journal*, 17:9, 2021, 23-31.
22. Daniel Navas, Sandra Fuentes, Alejandro Castro-Alvarez and Emigdio Chavez-Angel, “Review on sol-gel synthesis of perovskite and oxide nanomaterials”, *Gels*, 7, 2021, no. 4, 275.

23. Serena Esposito ““Traditional” sol-gel chemistry as a powerful tool for the preparation of supported metal and metal oxide catalysts”, *Materials*, 12, 2019, no. 4, 668.
24. Reyhaneh Nasr Azadani, Milad Sabbagh, Haniye Salehi, Amir Cheshmi, Ali Raza, Beena Kumari and Gisou Erabi, “Sol-gel: Uncomplicated, routine and affordable synthesis procedure for utilization of composites in drug delivery: Review”, *Journal of Composites and Compounds*, 3, 2021, no. 6, 57-70.
25. Swati Kumari, Sakshi Raturi, Saurabh Kulshrestha, Kartik Chauhan, Sunil Dhingra, Kovács András, Kyaw Thu, Rohit Khargotra, and Tej Singh, “A comprehensive review on various techniques used for synthesizing nanoparticles”, *Journal of Materials Research and Technology*, 27, 2023, 1739-1763.
26. Naima Zarrin, Shahid Husain, Wasi Khan, and Samiya Manzoor, “Sol-gel derived cobalt doped LaCrO<sub>3</sub>: structure and physical properties”, *Journal of Alloys and Compounds*, 784, 2019, 541-555.
27. M. Aamir, I. Bibi, S. Ata, K. Jilani, F. Majid, S. Kamal, N. Alwadai, M.A.S. Raza, M. Bashir, S. Iqbal, M. Aadil and M. Iqbal, “Ferroelectric, dielectric, magnetic, structural and photocatalytic properties of Co and Fe doped LaCrO<sub>3</sub> perovskite synthesized via micro-emulsion route”, *Ceramics International*, 47, 2021, no.12, 16696-16707.
28. Madzlan Aziz, Saad Saber Abbas, Wan Rosemaria Wan Baharom, and Wan Zuraidah Wan Mahmud, “Structure of SnO<sub>2</sub> nanoparticles by sol–gel method” *Materials Letters*, 74, 2021, 62-64.
29. Prashant Bhimrao Koli, Kailas Haribhau Kapadnis, Uday Gangadhar Deshpande, Umesh Jagannath Tupe, Sachin Giridhar Shinde, and Raju Shivaji Ingale, “Fabrication of thin film sensors by spin coating using sol-gel LaCrO<sub>3</sub> Perovskite material modified with transition metals for sensing environmental pollutants, greenhouse gases and relative humidity”, *Environmental Challenges*, 3, 2021, 100043.
30. Vrushali Shyamrao Shinde, Chatur Pundalik Sawant, and Kailas Haribhau Kapadnis, “Modified Sn-doped LaCrO<sub>3</sub> nanostructures: focus on their characterization and applications as ethanol sensor at a lower temperature”, *Journal of Nanostructure in Chemistry*, 9, 2019, 231-245.

31. M. A. Yakimchuk, E. S. Eliseeva and V. F. Kostyukov “Nanocrystalline films based on  $\text{YCrO}_3$  and  $\text{LaCrO}_3$  yttrium and lanthanum chromites doped with strontium ions  $\text{Sr}^{2+}$  as a basis for semiconductor gas sensors”, *Condensed Matter and Interphases*, 26, 2024, no. 3, 536-546.
32. Wenwen Zeng, Yingzhi liu, Jun Mei, Changyu Tang, Kun Luo, Shaomin Li, Haoran Zhan, and Zhoukun He, “Hierarchical  $\text{SnO}_2$ – $\text{Sn}_3\text{O}_4$  heterostructural gas sensor with high sensitivity and selectivity to  $\text{NO}_2$ ”. *Sensors and Actuators B: Chemical*, 301, 2019, 127010.
33. Vinay Kishnani, Gulshan Verma, Rohit Pippara, and Anshul Yadav, “Highly sensitive, ambient temperature CO sensor using tin oxide based composites”, *Sensors and Actuators A: Physical*, 332, 2021, 113111.
34. Satish Arvind Ahire, Prashant Bhimrao Koli, Arun Vitthal Patil, Bapu Sonu Jagdale, Ashwini Ashok Bachhav, and Thansing Bhavsing Pawar, “Designing of screen-printed stannous oxide ( $\text{SnO}_2$ ) thick film sensors modified by cobalt and nitrogen elements for sensing some toxic gases and volatile organic compounds”, *Current Research in Green and Sustainable Chemistry*, 4, 2021, 100213.
35. Sonali Wagh, Umesh Tupe, Anil Patil, and Arun Patil, “Influence of Annealing Temperature on Structural and Electrical Properties of Screen-Printed Lanthanum Oxide Thick Films”, *Iranian Journal of Materials Science & Engineering*, 19, 2022, no. 4, 1-9.
36. Vinayak R. Bagul, Ganesh Ramdas Bhagure, Satish A. Ahire, , Arun Vitthal Patil, Vishnu Adole , Prashat Bhimrao Koli “Fabrication, characterization and exploration of cobalt (II) ion doped, modified zinc oxide thick film sensor for gas sensing characteristics of some pernicious gases”, *Journal of the Indian Chemical Society*, 98, 2021, no. 11, 100187.
37. Sunil Jagannath Patil, Arun Vithal Patil, Chandrakant Govindrao Dighavkar, Kashinath Shravan Thakare, Ratan Yadav Borase, Sachin Jayaram Nandre, Nishad Gopal Deshpande and Rajendra Ramdas Ahire, “Semiconductor metal oxide compounds based gas sensors: A literature review”, *Frontiers of Materials Science*, 9, 2015, no. 1, 14-37.
38. Cheng Peng, Binwei Wang and Adrein Vincent, “ $\text{LaCrO}_3$ – $\text{VO}_x$ –YSZ anode material for solid oxide fuel cells operating on  $\text{H}_2\text{S}$ -containing syngas”, *Journal of Materials Science*, 47, 2012, 227-233.
39. Umesh Jagannath Tupe, Arun Vitthal Patil, Madhukar Sarvottam Zambare and Prashant Bhimrao Koli, “Stannous Oxide Thick Film Nanosensors Design by Screen Printing

Technology: Structural, Electrical Parameters and H<sub>2</sub>S Gas Detection Study”, *Material Science Research India*, 18, 2021, no. 1, 66-74.

40. Upendra D Lad, NS Kokode, Mangesh B Deore, and Umesh J Tupe, “MgO incorporated ZnO nanostructured binary oxide thin film ethanol gas sensor”, *IJSDR*, 6, 2021, no.1, 135-142.
41. Arun Patil, Chandrakant Dighavkar, Ratan Borse, Shriram Patil, Rajendra Khadayate, “Effect of Cr<sub>2</sub>O<sub>3</sub> by Doping and Dipping On Gas Sensing Characteristics of ZnO Thick Films”, *Journal of Electron Devices*, 15, 2012, 1274-1281.
42. Mansi H. Magar, Vishnu A. Adole, Manohar R. Patil, Ravindra H. Waghchaure, Umesh J. Tupe, and Thansing B. Pawar, “Fabrication of modified Sb<sub>2</sub>O<sub>3</sub> nanospheres for the removal of hazardous malachite green organic pollutant and selective NO<sub>2</sub> gas sensor”, *Journal of the Indian Chemical Society*, 101, 2024, no.11, 101396.
43. Umesh Jagannath Tupe, Madhukar Sarvottam Zambare, Arun Vitthal Patil, and Prashant Bhimrao Koli, “The binary oxide NiO-CuO nanocomposite based thick film sensor for the acute detection of Hydrogen Sulphide gas Vapours”, *Material Science Research India*, 17, 2020, no.3, 260-269.
44. Upendra D. Lad, Namdeo S. Kokode, and Umesh J. Tupe, “Study of pn Heterojunction Thin Films for Reducing Gas Sensing Application Fabricated by Thermal Evaporation Technique”, *Advanced Materials Research*, 1172, 2022, 67-82.
45. S. M. Khetre, C. J Khilare, V.S. Shivankar, and S. R. Bamane, “Preparation and Study of Acetone Gas Sensing Behavior of Nanocrystalline LaCrO<sub>3</sub> Thick Film”, *Sensors & Transducers*, 137, 2012, no.2, 165-175.
46. Vrushali Shyamrao Shinde, Kailas Haribhau Kapadnis, Chatur Pundalik Sawant, Prashat Bhimrao Koli and Rajendra Popat Patil, “Screen print fabricated In<sup>3+</sup> decorated perovskite lanthanum chromium oxide (LaCrO<sub>3</sub>) thick film sensors for selective detection of volatile petrol vapors.”, *Journal of Inorganic and Organometallic Polymers and Materials*, 30, 2020, 5118-5132.
47. M. A. Gondal, Q. A. Drmosh, T. A. Saleh, “Preparation and characterization of SnO<sub>2</sub> nanoparticles using high power pulsed laser”, *Applied Surface Science*, 256, 2010, no. 23, 7067-7070.

48. Pawan Chetri, and Amarjyoti Choudhury, "Investigation of optical properties of SnO<sub>2</sub> nanoparticles", *Physica E: Low-dimensional Systems and Nanostructures*, 47, 2013, 257-263.
49. Pawan S. Suryawanshi, Arun V. Patil, Gitesh G. Padhye, and Umesh J. Tupe, "Investigation the Influence of Calcination Temperature on Structural, Electrical and Gas Sensing Properties MnO<sub>2</sub> Thick Films" *Advanced Materials Research*, 1180, 2024, 67-81.
50. Prashat Bhimrao Koli, Kailas Haribhau Kapadnis, Uday Gangadhar Deshpande, Balaji Pandurang More and Umesh Jagannath Tupe, "Sol-gel fabricated transition metal Cr<sup>3+</sup>, Co<sup>2+</sup> doped lanthanum ferric oxide (LFO-LaFeO<sub>3</sub>) thin film sensors for the detection of toxic, flammable gases: a comparative study" *Material Science Research India*, 17,2020, 70-83.
51. Dong Shuying, Cui Lingfang, Liu Canyu, Zhang Fangyuan, Li Kuiying, Xia Longji, Su Xianfa, Feng Jinglan, Zhu Yongfa and Sun Jianhui, "Fabrication of 3D ultra-light graphene aerogel/Bi<sub>2</sub>WO<sub>6</sub> composite with excellent photocatalytic performance: A promising photocatalysts for water purification", *Journal of the Taiwan Institute of Chemical Engineers*, 97, 2019, 288-296.
52. Raju Shivaji Ingale, Sachin Giridhar Shinde, Kashmiri Ashish Khamkar, Prashant Bhimrao Koli, Sachin Arun Kulkarni and Ishwar Jadhav Patil, "Al<sup>3+</sup> impregnated photolithographically fabricated sensor material La<sub>2-x</sub>Al<sub>x</sub>ZnO<sub>4</sub>: structural investigation and acute gas sensing study for hazardous air pollutant gases and humidity assay", *Sensing and Imaging*, 25, 2024, no. 1, 36.
53. Ravindra Haribhau Waghchaure, Vishnu Ashok Adole, Bapu Sonu Jagdale, Prashat Bhimrao Koli, "Fe<sup>3+</sup> modified zinc oxide nanomaterial as an efficient, multifaceted material for photocatalytic degradation of MB dye and ethanol gas sensor as part of environmental rectification", *Inorganic Chemistry Communications*, 140, 2022, 109450.
54. Minakshi Dilip Birari, Ishwar Jadhav Patil, Satish Arvind Ahire, Sachin Giridhar Shinde, Prashant Bhimrao Koli and Raju Shivaji Ingale, "Ferroso-ferric oxide (Fe<sub>3</sub>O<sub>4</sub>) embedded g-C<sub>3</sub>N<sub>4</sub> nanocomposite sensor fabricated by photolithographic technique for environmental pollutant gas sensing and relative humidity characteristics." *Inorganic Chemistry Communications*, 146, 2022,110083.

55. G. Ramanathan, N. Srinivasan (Arunsankar) and K. R. Murali, "Detection of H<sub>2</sub>S gas sensing performance of sol gel prepared metal oxide (In<sub>2</sub>O<sub>3</sub>, SnO<sub>2</sub>, Sn doped In<sub>2</sub>O<sub>3</sub>) thin films", *materialstoday:PROCEEDINGS*, 92, 2023, no.2, 1218-1224.
56. Zhidong Lin, Na Li, Zhe Chen and Ping Fu "The effect of Ni doping concentration on the gas sensing properties of Ni doped SnO<sub>2</sub>", *Sensors and Actuators B: Chemical*, 239, 2017, 501-510.
57. Chenyi Yuan, Junhao Ma, Yidong Zou, Guisheng Li, Hualong Xu, Victor V Sysoev, Xiaowei Cheng and Yonghui Deng, "Modeling Interfacial Interaction between Gas Molecules and Semiconductor Metal Oxides: A New View Angle on Gas Sensing", *ADVANCED SCIENCE*, 9, 2022, no. 33, 2203594.